DESIGN OF AN INFRARED SYSTEM FOR MEASURING STAGNATION POINT HEAT TRANSFER RATES IN AN ELECTRO-MAGNETIC SHOCK TUBE

WILLIAM R. PHILLIPS
AND
LARRY G. VALADE

DESIGN OF AN INFRARED SYSTEM FOR MEASURING STAGNATION POINT HEAT TRANSFER RATES IN AN ELECTROMAGNETIC SHOCK TUBE

By

William R. Phillips
Lieutenant, United States Navy

and

Larry G. Valade
Lieutenant, United States Navy

Submitted in partial fulfillment of
the requirements for the degree of

MASTER OF SCIENCE
IN
ELECTRICAL ENGINEERING

United States Naval Postgraduate School
Monterey, California

1959

DESIGN OF AN INFRARED SYSTEM FOR MEASURING STAGNATION POINT HEAT TRANSFER RATES IN AN ELECTROMAGNETIC SHOCK TUBE

By

William R. Phillips

and

Larry G. Valade

This work is accepted as fulfilling

the thesis requirements for the degree of

MASTER OF SCIENCE

IN

ELECTRICAL ENGINEERING

from the

United States Naval Postgraduate School

ABSTRACT

Growing interest in the recovery of astrovehicles and artificial planets has led to investigations of surface cooling at hypervelocities (Mach numbers greater than 15). The simulation of these problems using models in electromagnetic shock tubes has offered a direct approach toward verification of predicted heat transfer rates. This thesis is an analysis of a proposed experimental apparatus which will measure the stagnation point heat transfer rate to models in highly ionized flows in the electromagnetic shock tube.

It is proposed that stagnation point temperature measurements be made with a photoconductive cell by measuring the infrared radiation emitted from a metallic (gold) film placed on a quartz window in the nose of the model. From the measured variation of temperature with time, the heat transfer rate can be determined. The transmission path of the infrared radiation is along a sapphire light pipe to a lead sulphide detector external to the model. The device is capable of operating under conditions where high ionization levels make the use of resistance film gages impractical, and it may also be operated in the presence of varying magnetic fields. The device is capable of detecting heat transfer rates between approximately 2000 and 35,000 Btu/ft^2-sec. The lower value is determined by the available period of observation (40 microseconds) while the upper value is limited by the detector cell time response, melting temperature of the gold film and the available period of observation. The response time of the system limits observation periods to those equal to or greater than the available minimum detector cell time constant (about

10 microseconds). Expected heat transfer rates are calculated and an optimum operating wavelength is derived. Component specifications are determined and calibration techniques are suggested.

The system concept and preliminary design work were originated by Dr. R. W. Ziemer at the Physical Research Laboratory, Space Technology Laboratories, Inc., Los Angeles, California. The system is presently being constructed and is expected to be in operation sometime in 1959. This analysis was made by Larry G. Valade, Lieutenant, U. S. Navy, and William Rees Phillips, Lieutenant, U. S. Navy, at the Physical Research Laboratory through the kindness of Dr. Milton U. Clauser, Director.

ACKNOWLEDGMENT

The authors are extremely grateful for the guidance and assistance given so freely by Dr. Ziemer. Mr. William Bush was most helpful in discussing certain aspects of the mathematical derivations. Mrs. Mildred Anderson's calculations and drawings, and Mrs. Goldie Sorkin's generous assistance with the manuscript, are especially appreciated and have aided greatly in the preparation of this paper.

TABLE OF CONTENTS

LIST OF ILLUSTRATIONS

LIST OF ILLUSTRATIONS (Continued)

TABLE OF SYMBOLS

A	Area
B	Magnetic field density, webers/meters^2
C	Electrical capacitance, farads
D	Differential operator
E	Electrical potential, volts
I	Current, amperes
K	Thermal diffusivity, ft^2/sec
M	Mach number
P	Power, watts, Btu/sec
R	Resistance (electrical), ohms
R	Responsivity, volts/watt
R	Reflectivity (optical)
R	Gas constant
S	Jones quantity
T	Temperature
T_i	Transmission efficiency
V	Volume
W	Emissive power, watts/cm^2-micron
a	Speed of sound, ft/sec
c	Velocity of light, cm/sec
c_p	Specific heat at constant pressure, Btu/lbm-°F
d	Film thickness, Å
f	Frequency, cycles/sec
h	Enthalpy, Btu/lbm
h	Planck's constant
i_c	Angle of incidence, degrees

k	Boltzmann's Constant
l	Length
p	Pressure, lbf/ft^2
q	Heat transfer rate, Btu/ft^2-sec
r	Energy ratio, Btu/Btu
s	Laplace variable
t	Time, seconds
u	Velocity, ft/sec

Greek

α	Absorption constant, cm^{-1}
α	Thermal coefficient of resistivity, $°K^{-1}$
γ	Specific heat ratio
ϵ	Emissivity
η	Index of refraction
κ	Thermal conductivity, Btu/sec-ft-°F
λ	Wavelength, microns
ρ	Density, lbm/ft^3
ρ	Resistivity, ohm-cm
σ	Stefan-Boltzmann constant
τ	Time constant, seconds
τ	Dummy variable of integration
ϕ	Magnetic flux, webers
ω	Frequency, rad/sec

Subscripts

c	Convection (heat transfer)
g	Gold film

o	Standard or reference condition
r	Radiation (heat transfer)
s	Shock wave
s	Signal
s	Stagnation point of model (enthalpy)
w	Shock tube wall stagnation (enthalpy)

1. Introduction.

With the current interest in space vehicles and re-entry heating, the problem of measuring the heat transfer rate to a blunt body in a highly ionized, magnetoaerodynamic flow has become increasingly important. A device is proposed for the measurement of the stagnation point heat transfer rate on a test model and was designed for use in the electromagnetic shock tube shown in Fig. 1. The basic concept consists of placing a thin metallic film on the nose of the model, shown in the shock tube in Fig. 2, and then observing the infrared radiation at a selected wave length with a photoconductive detector cell. The ultimate objective is to verify the magnetic cooling effect predicted by Meyer [1] and Bush [2]. This design is a continuation of the magnetoaerodynamic research work performed by Dr. R. W. Ziemer and W. B. Bush, Space Technology Laboratories, Los Angeles, California, in determining the magnetic field effects on hypervelocity flow about a blunt body [3].

Resistance film heat transfer gages have been utilized with a great deal of success for this type of measurement [4]. However, at the higher Mach numbers (above approximately 15), the ionized particles striking the resistance gage generate noise greater than the normal signal, making the system impractical for such flows.

Successful observations of explosion temperatures by photomultiplier color pyrometers [5] suggested radiometric measurement of the surface temperature of projectiles fired at hypervelocities. This method is being employed at the U. S. Naval Ordnance Test Station, China Lake, California, [6] utilizing electron photomultiplier tubes operating at wave lengths of 0.55 to 0.75 micron. The application

of this technique in the infrared spectrum to the magnetoaerodynamic heat transfer problem was suggested by Ziemer.

The problem of detecting infrared radiation from the model in a shock tube with an approximate stream temperature of 8000°K, and shock layer temperatures up to 35,000°K, presents many interesting considerations. In addition, the short duration of steady state conditions (15 to 40 microseconds), the necessity of shielding the detector cell from the free stream and shock layer radiation, and the need for electromagnetic shielding of the electronic components, places stringent requirements on the system.

Initial calculations indicated that model nose film temperatures from 300 to 1200°K could be expected. The wave length of peak radiation at these temperatures lies between two and ten microns. The greater sensitivity of lead sulphide cells (over other photoconductive detectors) will be required for maximum system response. Typical spectral response characteristics[7] of a lead sulphide cell are shown in Fig. 3. Peak response of this cell lies between 1.9 and 3.5 microns. The high temperature radiation from the free stream gases[8] exhibits an apparent minimum at a wave length of 3.1 microns. These considerations suggest an initial spectrum of interest between wave lengths of two and four microns.

In designing the system, the following will be considered,

(1) A study of the shock tube characteristics and evaluation of the expected heat transfer rates

(2) Selection of the metallic film material and thickness

(3) Determination of a suitable energy transmission path

(4) Selection of an optimum wave length

(5) Detector cell performance

(6) Instrumentation

(7) Calibration.

2. Conditions of Heat Transfer Measurements in the Electromagnetic Shock Tube.

In order to design a heat transfer measurement system it will be necessary to first examine those conditions under which the measurements will be made. It will be shown later that the system must be capable of measuring extremely high transfer rates up to 35,000 Btu/ft^2-sec. The measurements must be made within the 15 to 40 microsecond steady-state times inherent in electromagnetic shock tubes. The device must also be insensitive to strong electromagnetic radiation from the shock tube gases and the electrical circuitry.

The test model is shown in Fig. 2. The physical dimensions closely approximate those of models used in previous work with the shock tube. The operation of this particular shock tube has been described in detail by Ziemer. [9] The following basic principles are outlined for the reader unfamiliar with this device.

A high voltage electrical discharge at the base of the tube suddenly adds driving energy to a portion of the gas. As the gas rapidly expands, a simultaneous magnetic pinch forces the gas down the shock tube. A very strong shock wave with Mach numbers of 40 or more is generated. The main equipment associated with the tube consists of the shock tube assembly, electrical spark gap switch, high voltage power supply, condenser bank, trigger pulse circuitry, high current pulser for applying the magnetic field at the nose of the model, and a vacuum system for evacuating the tube. The complete system is shown schematically in Fig. 4.

Various shock tube operating conditions are obtained by evacuating the tube to various initial pressures in the range from 30 to 300 microns.

2. Conditions of Heat Transfer Measurements in the Electromagnetic Shock Tube.

In order to design a heat transfer measurement system it will be necessary to first examine those conditions under which the measurements will be made. It will be shown later that the system must be capable of measuring extremely high transfer rates up to 35,000 Btu/ft^2-sec. The measurements must be made within the 15 to 40 microsecond steady-state times inherent in electromagnetic shock tubes. The device must also be insensitive to strong electromagnetic radiation from the shock tube gases and the electrical circuitry.

The test model is shown in Fig. 2. The physical dimensions closely approximate those of models used in previous work with the shock tube. The operation of this particular shock tube has been described in detail by Ziemer. [9] The following basic principles are outlined for the reader unfamiliar with this device.

A high voltage electrical discharge at the base of the tube suddenly adds driving energy to a portion of the gas. As the gas rapidly expands, a simultaneous magnetic pinch forces the gas down the shock tube. A very strong shock wave with Mach numbers of 40 or more is generated. The main equipment associated with the tube consists of the shock tube assembly, electrical spark gap switch, high voltage power supply, condenser bank, trigger pulse circuitry, high current pulser for applying the magnetic field at the nose of the model, and a vacuum system for evacuating the tube. The complete system is shown schematically in Fig. 4.

Various shock tube operating conditions are obtained by evacuating the tube to various initial pressures in the range from 30 to 300 microns.

The tube is usually operated with air, but could be filled with any gas of interest. Shock Mach numbers are approximately inversely proportional to the initial tube pressure at the time of firing.

In order to fire the tube, a high voltage supply charges the capacitor bank to about 25 kilovolts, which is applied between the ring and lower spark gap electrodes. The spark gap prevents current flow until the 15-kilovolt pulse is applied to the lower switch plate. Then the voltage between the lower switch plate and the trigger wire exceeds the breakdown potential, and this initial discharge ionizes the gas in the spark gap, which becomes conductive. This permits the capacitors to discharge, and current flows from the center electrode to the ring electrode and down the six copper straps placed around the outside of the tube's conical section. The resulting high current produces a magnetic field which pinches and further heats the ionized gas in the cone, driving the shock wave down the tube.

A high current can be pulsed through the coil located in the nose of the model, resulting in maximum magnetic field strengths of about 40 kilogauss at the stagnation point. The current is supplied by an L-C circuit whose resonant frequency is approximately 2000 cps.

The shock tube is fired just prior to the time when the field strength is at its peak value. This provides an essentially constant magnetic field over the 40-microsecond test period due to the relatively long 500-microsecond period of the L-C pulsing circuit.

In order to determine the thermodynamic conditions existing in the tube, the shock wave velocity is measured experimentally by means of the rotating mirror camera. [10] Knowing the shock velocity

together with the initial pressure or density, is sufficient to calculate the characteristic properties of the flow.

The shock tube flow characteristics, free stream density ratio, ρ_2/ρ_o, and the free stream velocity, u_2, as functions of shock Mach number are determined as follows:

From the continuity equation,

$$\rho_1 u_1 = \rho_2 u_2$$

and from the diagrams of Fig. 5,

$$\frac{\rho_2}{\rho_1} = \frac{u_1}{u_2} = \frac{u_s}{u_s - u_2} = \frac{\frac{u_s}{a_1}}{\frac{u_s}{a_1} - \frac{u_2}{a_1}} = \frac{M_s}{M_s - \frac{u_2}{a_1}}$$

Let M_2' be defined as

$$M_2' = M_2 \sqrt{\frac{\gamma_2 T_2}{\gamma_1 T_1}} = \frac{u_2}{a_1}$$

then

$$(M_s - M_2') \rho_2/\rho_1 = M_s$$

$$M_2' = M_s (1 - \rho_1/\rho_2) = M_2 \sqrt{\frac{\gamma_2 T_2}{\gamma_1 T_1}}$$

Since

$$M_2 = \frac{u_2}{a_2}$$

then

$$\frac{u_2}{a_1} = M_2 \frac{a_2}{a_1} = M_2 \sqrt{\frac{\gamma_2 RT_2}{\gamma_1 RT_1}}$$

Utilizing the Hugoniot shock wave relationships and the thermodynamic properties of high temperature air reported by Gilmore, [11] the desired quantities are readily obtained for various shock tube initial conditions, and these are presented graphically in Fig. 6.

The operating characteristics of the shock tube using air may be summarized as follows:

Shock Mach number, M_s	15 to 40
Initial density ratio, ρ/ρ_o	3×10^{-4} to 3×10^{-5}
Free stream density ratio, ρ_2/ρ_o	3.6×10^{-3} to 6×10^{-4}
Free stream Mach number, M_2	2.9 to 3.9
Free stream velocity, u_2	15,000 to 41,000 ft/sec
Free stream temperature, T_2	6000 to 11,000°K
Shock layer temperature, T_1	20,000 to 35,000°K
Test duration	15 to 40 microseconds

Pressure shock tube experiments for determining the stagnation point heat transfer rate on similar test models have been reported by Detra [12] of the Avco Research Laboratory, Everett, Massachusetts. It was found that at test shock Mach numbers of up to 17, the following empirical relationship described the observed heat transfer rates.

$$q_s = \frac{17,600}{R} \sqrt{\rho_2/\rho_o} \left(\frac{u}{u_o}\right)^{3.15} \left(\frac{h_s - h_w}{h_s - h_{w300}}\right) \text{Btu/ft}^2\text{-sec}$$

where R is the body nose radius, u_o is taken as a reference velocity, 26,000 ft/sec, and h_w, and h_s, the wall and stagnation enthalpies, respectively.

Making the assumptions that,

$$h_s \gg h_w$$

$$h_s \gg h_{w300}$$

the expression reduces to

$$q_s = \frac{17,600}{R} \sqrt{\frac{\rho_2}{\rho_o}} \left(\frac{u}{u_o}\right)^{3.15} \text{ Btu/ft}^2\text{-sec}$$

Substitution of the previously determined thermodynamic properties into the equation above results in the heat transfer rate curve as a function of shock Mach number and is shown in Fig. 7. The validity of this relationship becomes suspect above the range of Detra's experimental verification, because it would seem that the radiation effects from the shock layer and free stream gases may be contributing substantially to the heat transfer rate. These effects are probably just becoming significant at the highest velocities observed by Detra.

It should be noted that the Detra equation is valid for atmospheric free stream or actual flight conditions and substituting values obtained in the electromagnetic shock tube into this expression will yield erroneous values. Free stream temperatures in the shock tube are about 8000°K, while actual flight stream temperatures will be of the order of 100°K and will vary with altitude density. When this was taken into

account, preliminary calculations indicated that the heat transfer rate in the shock tube will be approximately 25 per cent greater than that shown in Fig. 7.

An analytical study by Meyerott [13] reported the effect of radiation heat transfer is governed by the relation

$$q_r \sim \rho^{3/2} R u^{10}$$

while the convective heat transfer appears as

$$q_c \sim \rho^{1/2} R^{-1/2} u^3$$

The expression for convective heat transfer agrees closely with Detra's expression. However, a comparison of the two heat transfer rates, q_r and q_c, within the range of interest indicates that the radiative contribution is of the order of ten per cent or higher of the convective portion. This means that the estimated heat transfer rate in the shock tube will be greater than that calculated for pure convective heating. Hence, due to both the "artificial" conditions in the shock tube, and the radiative heat effects, the total heat transfer rate to the test body in the shock tube will be appreciably greater than that predicted by Detra's equation.

3. Thin Film Requirements.

Several factors must be considered in selecting the metallic film to be placed on the test body. A maximum temperature rise is desired in the short time available for measurement in order to obtain a high emissive power. This requires a film material of high thermal diffusivity, evaporated on a substrate of low thermal diffusivity. Moreover, the film should be of minimum thickness so that the temperature gradient within the film will be small.

The emitted radiation from the film must be observed from behind the film so that the observed radiation does not have to pass through the hot and also radiating gases in the free stream and shock layer. However, thin metallic films may permit appreciable transmission of radiant energy [14] in the spectrum of interest. In order to have the film opaque to this radiation, the film should have a high reflectivity, a high absorption coefficient and a certain minimum thickness. Therefore, because of conflicting thermal and optical requirements, a compromise film thickness must be determined.

Thermal and optical properties of various film and substrate materials must be considered. The desirability of a gold film and a quartz substrate is evident from examination of the properties of the most promising materials listed below.[1]

The chemical inertness of gold is another factor that makes its use attractive. Certain grades of quartz are opaque above wave lengths of 2.5 microns, but selected fuzed quartz has excellent transmission out to about 4 microns. [15]

[1] These properties and those physical constants used throughout the thesis were largely obtained from American Institute of Physics Handbook, McGraw-Hill, New York, 1957.

Material	Thermal Diffusivity ft^2/sec	Specific Heat Btu/hr-ft-°F	Spectral Emissivity 2-4μ	Absorption Coefficient 2-4μ cm^{-1}
Gold	12.64×10^{-4}	0.031	0.03	20.0
Platinum	2.72×10^{-4}	0.032	0.03	3.4
Quartz	9.00×10^{-6}	0.18	--	--
Pyrex	7.00×10^{-6}	0.20	--	--
Sapphire	9.77×10^{-5}	0.18	0.03	--

The transmissivity of the gold film must be investigated in order to determine an optimum thickness which will permit a minimum temperature gradient from the outer to the inner film face, and a maximum ratio of emitted film radiation to transmitted hot gas radiation. The transmitted energy is made up of radiation from both the free stream and shock layer gases and may be expressed in terms of the incident radiant energy on the gold film as

$$W_t = (W_1 + W_2)(1 - R) \exp\left[-2\pi a \frac{d}{\lambda}\right]$$

where R is the reflectivity constant, a, the absorption coefficient and d, the film thickness.

The ratio of the emitted energy to the transmitted energy for all wave lengths may be expressed in terms of Planck's Law as,

$$\frac{W_g}{(W_2 + W_1)(1 - R)\exp\left[-2\pi a \frac{d}{\lambda}\right]} =$$

$$\frac{\epsilon_g 2\pi c^2 h \int_{\lambda_1}^{\lambda_2} \frac{d\lambda}{\lambda^5 \exp\left[\frac{ch}{k\lambda T}\right] - 1}}{\left[\epsilon_2 2\pi c^2 h \int_{\lambda_1}^{\lambda_2} \frac{d\lambda}{\lambda^5 \exp\left[\frac{ch}{k\lambda T_2}\right] - 1} + \epsilon_1 2\pi c^2 h \int_{\lambda_1}^{\lambda_2} \frac{d\lambda}{\lambda^5 \exp\left[\frac{ch}{k\lambda T_1}\right] - 1}\right](1 - R)\exp\left[-2\pi a \frac{d}{\lambda}\right]}$$

For a single wave length, the above equation reduces to

$$\frac{W_g}{W_t} = \frac{\epsilon_g / \exp\left[\frac{ch}{k\lambda T}\right] - 1}{\epsilon_{1,2}\left[\frac{1}{\exp\left[\frac{ch}{k\lambda T_2}\right] - 1} + \frac{1}{\exp\left[\frac{ch}{k\lambda T_1}\right] - 1}\right](1 - R)\exp\left[-2\pi a \frac{d}{\lambda}\right]}$$

Assuming black body radiation from the gases,

$$\epsilon_{1,2} = \epsilon_1 = \epsilon_2 = 1$$

Substituting the value of

$$\epsilon_g = 0.03 \quad \text{for} \quad 2\mu < \lambda < 5\mu$$

and then evaluating the energy ratio as a function of λ for various thickness with

T_1 = 35,000°K

T_2 = 8000°K

R = 0.983

a = $f(\lambda)$ from Fig. 8

yields the curves of Fig. 9. This graph indicates that a thickness of 5000 Å gives a ten to one ratio of emitted energy to transmitted energy for wave lengths of interest.

The temperature profile in the substrate for a 5000 Å thick film is determined next as a function of time and heat transfer rate. The differential equations describing the heat flow are well known and the solution has appeared in several references. [16], [17] The method of solving the problem is to first assume the thin film to be a semi-infinite slab as shown in Fig. 10. The solution to this configuration is later used in the exact solution for a film of finite thickness on a substrate of different thermal properties. The differential equation describing this temperature rise-time relationship in the semi-infinite slab is

$$\frac{\partial \theta}{\partial t} = K \frac{\partial^2 \theta}{\partial x^2} \quad \text{for} \quad \theta(x, t)$$

where

$$K \equiv \frac{\kappa}{c_p \rho}$$

$$\theta(x, t) \equiv T(x, t) - T(x, o)$$

and

$T(x, t) \equiv$ temperature at any point, x, in the slab at time, t

The boundary conditions to be satisfied are

$$\theta(x, o) = 0 \tag{1}$$

$$\lim_{x \to \infty} \theta(x, t) = 0 \tag{2}$$

for $t > 0$

$$\left.\frac{\partial \theta}{\partial x}\right|_{x=0} = -\frac{q}{\kappa} \tag{3}$$

Using Laplace transform methods,

$$L(\theta) = \Theta(s)$$

then

$$s\Theta = K\frac{d^2\Theta}{dx^2}$$

$$\Theta\left(D^2 - \frac{K}{s}\right) = 0$$

and

$$\Theta(s) = c_1 \exp\left[\sqrt{\frac{K}{s}}\, x\right] + c_2 \exp\left[\sqrt{\frac{K}{s}}\, x\right]$$

Applying boundary conditions (2) and (3) to evaluate constants c_1 and c_2, it is found that

$$c_1 = 0$$

and

$$\left.\frac{d\Theta}{dx}\right|_{x=0} = -\frac{q}{\kappa}\left(\frac{1}{s}\right) = -c_2\sqrt{\frac{K}{s}}$$

giving

$$c_2 = \frac{q\sqrt{K}}{\kappa}\, s^{-3/2}$$

$$\therefore \Theta(s) = \frac{q\sqrt{K}}{\kappa}\, s^{-3/2} \exp\left[-\sqrt{\frac{K}{s}}\, x\right]$$

Taking the inverse transform, [18] the solution is

$$\theta(x,t) = \frac{q\sqrt{K}}{\kappa}\left[2\sqrt{\frac{t}{\pi}} \exp\left[-1/4\,\frac{x^2}{KT}\right] - \frac{x}{\sqrt{K}}\ \operatorname{erfc}\left(\frac{1}{2}\,\frac{x}{\sqrt{K}}\sqrt{\frac{1}{t}}\right)\right]$$

This temperature rise-time versus depth relationship is shown graphically in Fig. 11 for the general case, and the surface temperature solution is plotted in Fig. 12. If the properties of the substrate are used in this solution, the approximate solution is obtained for a very thin film on a semi-infinite substrate, for which the presence of the film has negligible effect.

However, the solution to the particular problem of a thin film of finite thickness mounted on a semi-infinite slab, as shown in Fig. 13, remains to be determined. One solution to this temperature rise-time relationship [19] is

$$\psi(x_1, t) = \frac{1}{\sqrt{\pi}} \frac{\sqrt{K}}{\kappa} \int_o^t \frac{q(\tau)}{\sqrt{t - \tau}} \exp\left[- \frac{x_1^2}{4K(t - \tau)} \right] d\tau$$

$$+ \sum_{n=1}^{\infty} b^n \left[\theta(2n\ell - x_1, t) + \theta(2n\ell + x_1, t) \right]$$

where

$$\psi(x_1, t) \equiv \text{temperature rise at any point, } x_1, \text{ in the film at time } t$$

and

$$b_n \equiv \frac{1 - a}{1 + a}$$

$$a \equiv \frac{\kappa_{\text{substrate}}}{\kappa_{\text{film}}} \sqrt{\frac{K \text{ film}}{K \text{ substrate}}}$$

It can be shown algebraically that

$$\theta(x, t) = \frac{1}{\sqrt{\pi}} \frac{\sqrt{K}}{\kappa} \int_o^t \frac{q(\tau)}{\sqrt{t - \tau}} \exp\left[- \frac{x_1^2}{4K(t - \tau)} \right] d\tau$$

where $\theta(x, t)$ is the previous solution for the semi-infinite slab of the film material.

For evaluation of the interface temperature rise as a function of time

$$x_1 = \ell$$

then, simplifying the general expression yields

$$\psi(\ell, t) = \sum_{n=1}^{\infty} b^{n-1} (1 + b)\, \theta\left[(2n - 1)\ell, t\right]$$

The outer face temperature rise may be expressed as

$$\psi(0, t) = \theta(0, t) + 2 \sum_{n=1}^{\infty} b^n\, \theta(2n\ell, t)$$

Evaluating the general expression for the 5000 Å thick gold film on a quartz substrate for various heat transfer rates, and assuming a room temperature of 300°K, gives the interface temperature versus time curves of Fig. 14.

4. Method of Radiation Transmission.

The problem of transmitting the radiated energy from the gold film to the infrared detector cell will be considered next. Knowing the characteristics of a typical detector cell, [7] the minimum detectable power level which must fall on the sensitive area of the detector can be determined. The temperature-time history of the film interface is known for the shock tube operating conditions, and therefore the power emitted by the film through the quartz substrate is also known.

The transmission problem, then, is to determine whether

$$W_g \times T_i \geq P_{detectable}$$

in which W_g = emissive power from the gold film

T_i = transmission efficiency of the system

$P_{detectable}$ = minimum power detectable by infrared cell

The problem is reduced to choosing a method of transmission with sufficient efficiency such that the lower limit established by

$$T_i > \frac{P_{detectable}}{W_g}$$

is exceeded or that T_i closely approaches 100 per cent.

The efficiency of any transmission system will be a function of the wave length of the transmitted energy. The operating wave length remains to be selected at a later stage of the analysis, and, therefore, no valid approximation is available for a probable value of T_i for a particular method. Therefore, the optimum transmission efficiency of a number of possible transmission methods will be examined, making the problem one of choosing the most efficient technique.

The first transmission system considered is an optical lens arrangement which will focus the emitted energy and direct it to the detector's sensitive area. Various lens-mirror arrangements were considered and it was found that the maximum transmission efficiency of any optical system is about 13 per cent. The geometry of the aerodynamic body restricts the efficiency of this method by limiting the collecting area of the first lens in the system.

The successful use of a sapphire rod as a light pipe, in silicon crystal growth control, [20] suggested a similar application to this problem. A study of the optical properties of crystals in the infrared region indicated that the transmissivity of sapphire, in thin samples, approaches 90 per cent for wave lengths up to approximately five microns. The proposed transmission system incorporating a sapphire light pipe is shown in Fig. 15. Based on this diagram, the transmission efficiency of the rod may be expressed as

$$T_{rod} = 2\int_{o}^{\pi/2} \cos\beta \exp\left[-\alpha L \sec i\right] di$$

in which L = length of the rod. From Snell's Law for the refraction of light

$$\frac{\sin\beta}{\sin i} = \frac{\eta_2}{\eta_1}$$

in which η is the spectral refractive index of the transmitting material. Then

$$T_{rod} = 2\int_{o}^{\pi/2} \sqrt{1 - \left(\frac{\eta_2}{\eta_1}\right)^2 \sin^2 i} \exp\left[-\alpha L \sec i\right] di$$

A lower bound for the transmission efficiency can be determined by evaluating the expression

$$T_{rod} \geq 2 \int_{o}^{i_c} \sqrt{1 - \left(\frac{\eta_2}{\eta_1}\right)^2 \sin^2 i} \exp\left[-\alpha L \sec i\right] di$$

where the angle, i_c, is that angle below which total reflection occurs.

The spectral coefficient, α, for sapphire appears in Fig. 16. The integral above was solved graphically over a range of wave lengths of two to five microns, and the results plotted in Fig. 17.

It is interesting to note that the use of the quartz substrate improved the transmission efficiency of the system. The refractive index of quartz is sufficiently less than that for sapphire so as to provide a focusing effect that permits more energy to fall on the face between the substrate and the light tube.

This study showed that a sapphire light pipe is a highly efficient means of transmitting energy in the infrared spectrum. The expected transmission efficiency of this configuration can be as high as 95 per cent in the near infrared and hence, the light pipe was selected in preference to the lens system.

5. Comparison of Infrared Signal and Extraneous Radiation.

The intensity of the signal power from the gold film received at the cell must be compared to the incident power emitted by all other sources. At the lower wave lengths, considerable power is transmitted through the film from the shock tube gases. At the longer wave lengths, power comparable to the signal power is emitted by the light pipe, substrate, and the test model walls. Hence, an optimum operating wave length will be determined to maximize the ratio of the signal power to the extraneous power. This investigation will require selection of the physical dimensions of the apparatus as it is mounted on the shock tube.

The diameter of the sapphire light pipe should be a maximum, in order to achieve greater transmission efficiency. However, this dimension is limited by the available space within the magnetic coil core. Further a small diameter is desirable to minimize the rod surface area, and, therefore, reduce the incident transverse power into the rod. Furthermore, it is advantageous to have the gold film diameter the same as the light pipe diameter. However, a minimum gold film area is required in order to approximate closely the stagnation point conditions. As a compromise, a diameter of 0.15 inch was selected for the initial assembly and subsequent calculations will be based on the resulting area for the gold film, substrate, sapphire rod, and infrared components.

The detail design of the test apparatus is shown in Fig. 18. The housing above the model will be utilized for the detector cell, circuitry, and other necessary electronic components. The housing is made of thick copper walls in order to shield the electrical components of the

system from stray electromagnetic radiation. The 3/16-inch minimum thickness used will permit penetration of only two per cent of 5000-cps radiation.

Returning to the problem of maximizing the signal to background power ratio, it will be necessary to investigate all possible sources of infrared radiation that will be incident on the cell, and if possible, to select a restricted spectral band in which the ratio of the emitted power from the gold film to the emitted power of all other sources will be a maximum. An interference filter will be required to limit the cell spectral response to a discrete bandwidth, permitting an optimum signal to background power ratio. Possible sources of undesirable noise radiation will include,

(1) Substrate

(2) Interference filter

(3) Incident heat flux on the model's structural surfaces, other than at the stagnation point

(4) Eddy current heating of the film by the magnetic field

(5) Light tube

(6) Free stream gases

(7) Shock layer gases

Sources 1 and 2 are negligible when the magnitude of emissivity is considered for thin layers of quartz and germanium. The radiation level from these sources remains at room temperature throughout the test period as indicated by Fig. 11.

The structural source level 3, is small, limited by the shielding effect of the copper and will be minimized by highly polishing the tube

surrounding the sapphire rod. Also the outer surface of the model will be fabricated with an opaque plastic material.

The heating of the gold film by the eddy currents induced by the magnetic field, is investigated and the magnitude of the temperature rise determined. The physical picture of the effect is illustrated in Fig. 19. The energy dissipated in the film can be determined by assuming a uniform flux density over the entire film of

$$\phi = A B_m \sin \omega t$$

and using the basic relationships

$$E = \frac{d\phi}{dt}$$

$$dP = \frac{E^2}{R}$$

$$R = \frac{\rho L}{A}$$

From the geometry of Fig. 19, the dissipative power is

$$P = \int_o^{r=D/2} \frac{d\pi\omega^2 B_m^2 \cos^2 \omega t\, r^3\, dr}{2\rho} = \frac{d\pi\omega^2 B_m^2}{8\rho}\left(\frac{D}{2}\right)^4 \cos^2 \omega t$$

evaluated for

$$B_m = 4 \text{ webers/sq meter}$$

$$\omega \doteq 1.05 \times 10^4 \text{ rad/sec}$$

$$D/2 = 0.075 \text{ in.}$$

$$\rho = 2.42 \ \mu\text{ohm - cm}$$

yielded

$$P = 0.19 \cos^2 \omega t \text{ watts}$$

The temperature rise in the film was estimated by means of the relation

$$c_p \rho V \Delta T = \int_0^{t_1} P \, dt$$

where $t_1 = 600 \mu$ sec, which resulted in

$$\Delta T \doteq 4.1 \times 10^{-4} \, ^\circ K/\text{cycle}$$

which can be ignored.

The sapphire rod, while nearly transparent to infrared radiation, has an emissivity comparable to that of the gold film in the spectrum of interest. This room temperature radiation from the sapphire rod is significant at the longer wave lengths and must be considered in choosing an optimum operating wave length. Using the familiar expression,

$$T_{rod} + \epsilon_{rod} + \alpha_{rod} = 1$$

and assuming

$$\alpha_{rod} = 0$$

then,

$$\epsilon_{rod} = (1 - T_{rod})$$

where

$$\epsilon_{rod} = f(\lambda)$$

from which the emitted power of the sapphire rod at 300°K may be expressed as

$$W_{rod} = 2\pi c^2 h \int_{\lambda_1}^{\lambda_2} \frac{d\lambda (1 - T_{rod})}{\lambda^5 \exp\left[\frac{ch}{300k\lambda}\right] - 1}$$

Radiation from the sources 6 and 7 will be transmitted through the film as a function of film thickness and wave length as discussed in Sect. 3. This energy will be significant at the shorter wave lengths and, therefore, should be considered in arriving at an optimum wave length for system operation. For a film thickness of 5000 Å, and, assuming

$$\epsilon_2 = \epsilon_1 \equiv \epsilon_{12} = 1$$

$$T_2 = 8000°K$$

$$T_1 = 20{,}000°K$$

$$\alpha = f(\lambda)$$

$$R = 0.983$$

the radiation from the gases which is transmitted through the gold film can be expressed by

$$W_{12} = \epsilon_{12} 2\pi c^2 h \left[\int_{\lambda_1}^{\lambda_2} \frac{d\lambda}{\lambda^5 \exp\left[\frac{ch}{8000k\lambda}\right] - 1} + \int_{\lambda_1}^{\lambda_2} \frac{d\lambda}{\lambda^5 \exp\left[\frac{ch}{20{,}000k\lambda}\right] - 1} \right] (1 - R) \exp\left[-2\pi\alpha \frac{d}{\lambda}\right]$$

The selection of an optimum wave length will depend on evaluating the ratio

$$\frac{W_g(\lambda, T)}{W_{12}(\lambda) + W_{rod}(\lambda)} \equiv r(\lambda, T)$$

at different wave lengths and various temperatures, then determining that wave length which gives

$$r(\lambda, T) = r_{max}$$

The results of this computation clearly indicate, in Fig. 20, an optimum signal at

$$\lambda = 3\mu$$

The selection of a proper bandwidth is made by comparing the spectral response of the detector in Fig. 3 with the curves of Fig. 20. A wide bandwidth is desirable in order to have maximum incident power on the cell. However, a narrow bandwidth is required to obtain a high quality signal so that the ratio, r, is greater than some arbitrary value corresponding to a satisfactory signal-to-noise ratio.

It seems appropriate to select a bandwidth

$$\Delta\lambda \doteq 0.4\mu$$

centered at

$$\lambda \doteq 2.8\mu$$

in order to take advantage of maximum detector response. An interference filter, with characteristics as shown in Fig. 21, will be placed in front of the detector cell. This will limit the shorter wave length response, and the detector cell will limit the longer wave length response.

The power ratio,

$$r = \frac{W_g}{W_{12} + W_{rod}}$$

is evaluated at

$$\lambda = 2.8\mu$$

as a function of the gold film temperature and plotted on Fig. 22. This indicates that a film temperature of 380°K will be required in order to achieve a signal with

$$r > 6$$

The incident signal power on the detector from the gold film may be calculated from the temperature-time relationships in Fig. 14 by the following approximation:

$$W_g\Big|_{\substack{\text{on}\\\text{detector}}} = \frac{\epsilon_g 2\pi c^2 h}{\lambda^5 \exp\left[\frac{ch}{k\lambda T}\right] - 1} \cdot \Delta\lambda \cdot A \cdot T_{rod} \cdot T_{filter}$$

where

$$\Delta\lambda = 0.4\mu$$

$$A = 0.1152 \text{ cm}^2$$

$$T_{rod} = 0.8$$

$$T_{filter} = 0.3$$

$$\lambda = 2.8\mu$$

This equation is evaluated for three different heat transfer rates and the results appear graphically in Fig. 23.

Steady-state flow conditions are reached in the shock tube about five microseconds after the tube is fired. In order that the emissive power at this time be detected, the cell must be capable of sensing a minimum incident signal power of 0.015 microwatts for low shock Mach numbers.

6. Detector Cell Performance and Instrumentation.

Having determined the variation and amplitude of the incident radiation on the detector cell, the ability of an infrared cell to detect this aperiodic signal will be investigated next. A study of response characteristics of infrared cells indicated that lead sulphide cells have a superior relative response[21] in the spectrum of interest when compared with cells made up of other photoconductive materials such as lead telluride, lead selenide, and indium antimonide.

Before considering the minimum detectable signal of a cell, it will be helpful to define certain terms associated with infrared detector application. Noise-equivalent-power, P, is defined as that incident radiation on the cell which produces a signal to noise power ratio of unity[7] Another basic parameter, the "Jones quantity," S, is defined at some arbitrary reference level by the following relationship, [22]

$$S \equiv \frac{P}{\left(A \ln \frac{f_2}{f_1}\right)^{1/2}}$$

in which A = sensitive cell area and f_2 and f_1, are the upper and lower amplifier bandwidth half-power frequencies, respectively. The time constant, τ, is defined as the time required for the response to a step input to build up to 63 per cent of its maximum value and it has been observed that

$$S\tau = \text{constant} = C$$

Combining these two equations yields the somewhat simpler and more useful expression for noise-equivalent-power,

$$P = \frac{C}{\tau}\left(A \ln \frac{f_2}{f_1}\right)^{1/2}$$

Noise-equivalent-power is generally presented graphically as a function of wave length, as in Fig. 3, for specified reference values of τ, A, f_2 and f_1. By combining

$$P_o = \frac{C}{\tau_o}(A_o)^{1/2}\left(\ln \frac{f_2}{f_1}\right)_o^{1/2}$$

and

$$P^* = \frac{C}{\tau^*}(A^*)^{1/2}\left(\ln \frac{f_2}{f_1}\right)^{*1/2}$$

where the subscript, "o", applies to the standard reference condition and the superscript, "*", identifies those values for a particular cell-amplifier application. The noise-equivalent-power for a particular cell can be evaluated, when τ^*, A^*, f_2^* and f_1^* have been determined for proper signal output, by the expression

$$P^* = P_o\left(\frac{\tau_o}{\tau^*}\right)\left(\frac{A^*}{A_o}\right)^{1/2}\left[\frac{(\ln f_2/f_1)^*}{(\ln f_2/f_1)_o}\right]^{1/2}$$

Thus, the noise-equivalent-power, or minimum detectable signal power, is directly proportional to the square roots of the cell sensitive area and the logarithmic frequency ratio. The quantity is inversely proportional to the time constant. In order to evaluate the noise-equivalent-power, it will be necessary to investigate the bandwidth and time constant required to develop a meaningful signal across the detector cell. The majority of military and commercial applications

involve modulating the incident radiation as it strikes the detector and observing the entire spectrum of the emission source which is visible to the cell. Literature and manufacturers' data are presented with these applications in mind and, as a consequence, a special analysis will be required to determine the desired cell characteristics for this pulse input application.

The bandpass required to amplify the signal without excessive distortion will be determined first. The cell input signal as a function of time corresponding to

$$q = 5000 \text{ Btu/ft}^2\text{-sec}$$

has been selected for design purposes. This signal is approximated by the parabola shown in Fig. 24 and can be expressed as

$$f(t) = 0 \qquad t \leq 0$$

$$f(t) = 625\, t^2 \qquad 0 \leq t < 40 \times 10^{-6} \text{ sec}$$

$$f(t) = 0 \qquad t \geq 40 \times 10^{-6} \text{ sec}$$

Then, by means of the familiar Fourier integral relations, [23]

$$f(t) = \int_{-\infty}^{\infty} g(\omega)\, d\omega\, e^{j\omega t}$$

$$g(\omega) = \frac{1}{2\pi} \int_{-\infty}^{\infty} f(t)\, dt\, e^{-j\omega t}$$

it is possible to determine the magnitude of the frequency response as a function of frequency, from which the required amplifier bandwidth

is determined. A minimum bandwidth is desired in order to achieve minimum noise-equivalent-power. Proceeding then,

$$g(\omega) = \frac{1}{2\pi}\int_{-\infty}^{o} f(t)\,dt\,e^{-j\omega t} + \frac{1}{2\pi}\int_{o}^{40\times10^{-6}} f(t)\,dt\,e^{-j\omega t}$$

$$+ \frac{1}{2\pi}\int_{40\times10^{-6}}^{\infty} f(t)\,dt\,e^{-j\omega t}$$

$$= \frac{1}{2\pi}\int_{o}^{40\times10^{-6}} f(t)\,dt\,e^{-j\omega t}$$

For $a = 40 \times 10^{-6}$ sec, the approximate test duration in the shock tube, we obtain

$$\frac{2\pi}{625}\,g(\omega) = e^{-ja\omega}\left[\frac{2a}{\omega^2} + j\left(\frac{a^2}{\omega} - \frac{2}{\omega^3}\right)\right] + j\,\frac{2}{\omega^3} = \frac{2a}{\omega^2}\cos a\omega$$

$$+\left(\frac{a^2}{\omega} - \frac{2}{\omega^3}\right)\sin a\omega$$

$$+ j\left[\frac{2}{\omega^3} - \frac{2a}{\omega^2}\sin a\omega + \left(\frac{a^2}{\omega} - \frac{2}{\omega^3}\right)\cos a\omega\right]$$

If

$$R(\omega) = \frac{2a}{\omega^2}\cos a\omega + \left(\frac{a^2}{\omega} - \frac{2}{\omega^3}\right)\sin a\omega$$

$$I(\omega) = \frac{2}{\omega^3} - \frac{2a}{\omega^2}\sin a\omega + \left(\frac{a^2}{\omega} - \frac{2}{\omega^3}\right)\cos a\omega$$

then

$$\left|g(\omega)\right| = \frac{625}{2\pi}\sqrt{R^2(\omega) + I^2(\omega)}$$

Nondimensionalizing by means of

$$\frac{|g(\omega)|}{\lim_{\omega \to o} |g(\omega)|} \equiv |G(\omega)|$$

where

$$\lim_{\omega \to o} g(\omega) = \left(\frac{625}{2\pi}\right)\left(\frac{a^3}{3}\right)$$

and expressing $|G(\omega)|$ in decibels permits a simpler form in which to evaluate the frequency response for

$$1 \leq \omega \leq 10^6 \text{ rad/sec}$$

which is shown in Fig. 25. The magnitude is down 20 db at

$$f_2 = 15 \text{ kc}$$

which defines a conservative upper frequency limit for the amplifier.

Representing the signal as a single pulse is somewhat misleading. However, an exact solution would have entailed rather tedious computations not commensurate with the desired accuracy. Inasmuch as the system is eventually expected to be used in longer duration shock tubes, a wider bandwidth,

$$f_2^* = 50 \times 10^3 \text{ cps}$$

$$f_1^* = 0$$

will be utilized. Since the term in the noise-equivalent-power expression, $\ln(f_2/f_1)$, becomes indeterminate as f_1 approaches zero, the approximation,

$$f_1^* \doteq 10^{-4} \text{ cps}$$

will be made for design considerations.

The next characteristic to be investigated is the effect of the cell time constant on the detector output signal. It should be noted that the cell time constant and the noise-equivalent-power are extremely sensitive to cell temperature, exhibiting the following characteristics:[7]

Cell Temperature	Time Constant (microseconds)	Noise-Equivalent-Power (watts)
25°C	10 to 1000	P_o, say
75°C	2 to 200	$\approx 10\ P_o$
-78°C	100 to 10,000	$\approx 0.3\ P_o$
-196°C	200 to 10,000	$\approx 0.16\ P_o$

A minimum time constant can be achieved by heating the cell, but this increases the noise-equivalent-power, reducing the cell sensitivity. The input radiation signal is assumed as before to be

$$f(t) = 625\,t^2 \qquad 0 \leq t < 40 \times 10^{-6} \text{ sec}$$

$$f(t) = 0 \qquad \text{for all other } t$$

and a transfer function for the cell is assumed to be of the form,

$$H(s) = \frac{1}{1 + s\tau}$$

where s is the Laplace variable. Then, using Laplace transforms, the output signal can be expressed as

$$L\left[o(t)\right] = \left\{\left(\frac{1}{1 + s\tau}\right) L\left[f(t)\right]\right\}$$

$$L\left[f(t)\right] = F(s)$$

$$L\left[o(t)\right] = O(s)$$

$$F(s) = \frac{1250}{s^3}$$

$$O(s) = H(s)\,F(s)$$

$$= \frac{2 \times 625}{\tau}\left[\frac{1}{s^3(s + 1/\tau)}\right]$$

$$o(t) = f(t) - 1250\tau\left[t - \tau(1 - e^{-t/\tau})\right]$$

The output signal is determined for values of τ = 1, 5, and 10 microseconds and is plotted in Fig. 26. It is indicated by these curves that a minimum time constant is desirable, preferably less than five microseconds. This precludes the use of detector cooling and suggests heating the cell. However, heating the detector will provide an additional source of radiation that will be comparable to that emitted by the film, so the alternative of operating with an expected time constant of ten microseconds at room temperature must be accepted. Certain manufacturers have suggested the possibility of reducing this value of τ by a selection process and an attempt to procure a minimum time constant cell should be made.

For this analysis, the time constant will be assumed to be

$$\tau = 10 \text{ microseconds}$$

The sensitive cell area will be taken as that of the light tube,

$$A = 0.1152 \text{ cm}^2$$

Having determined the three basic parameters, it is now possible to evaluate the expected noise-equivalent-power based on the reference values in Fig. 3.

$$P^* = P_o \left(\frac{\tau_o}{\tau^*}\right)\left(\frac{A^*}{A_o}\right)^{1/2}\left[\frac{(\ln f_2/f_1)^*}{(\ln f_2/f_1)_o}\right]^{1/2}$$

$$= 3 \times 10^{-12}\left(\frac{180}{10}\right)\left(\frac{0.1152}{0.01}\right)^{1/2}\left[\frac{\left(\ln \frac{50 \times 10^3}{10^{-4}}\right)}{\left(\ln \frac{1005}{995}\right)}\right]^{1/2}$$

$$= 8.5 \times 10^{-9} \text{ watts}$$

This value indicates that an acceptable signal to noise ratio of the cell of six is reached at time

$$t \doteq 6 \text{ microseconds}$$

when the film temperature

$$T \doteq 360°K$$

However, a signal which is distinguishable from the background radiation is not available until $r = 6$, at which time

$$T \doteq 380°K$$

$$t \doteq 8 \text{ microseconds}$$

Steady state conditions in the shock tube are reached at about this same time, so this means that the period of observation should begin at

$$t \doteq 10 \text{ microseconds}$$

The magnitude of the output signal from the cell will be determined next. This quantity is commonly called responsivity and is expressed in units of output volts per watt of incident radiation. The cell is placed in a series circuit as shown in Fig. 27. Closing and opening the switch just before and after each test run will permit use

of maximum voltage across the detector without excessive heating of the cell. A high bias voltage gives the greatest signal. Hence, an applied battery voltage of 400 volts will be used, which is a practical upper limit.

A series resistor is used to match the cell resistance for maximum power delivery to the amplifier. The cell resistance varies somewhat with manufacture and will be assumed to be one megohm, which is a representative value. The signal from the detector is generated by the change in cell conductivity caused by the incident photons.

The responsivity varies with cell area, cell resistance, cell voltage, cell temperature, time constant, modulating frequency, and source temperature. The responsivity of an individual cell is usually determined by experimental means at some standard conditions. The data from such tests for a typical lead sulphide cell are presented in Fig. 28. The tests consist of focusing the radiation from a constant temperature black body source on the cell sensitive area. The temperature can be set at any desired level and the black body emitted power is distributed over the spectrum in accordance with Planck's spectral distribution law. Since the cell only responds to radiation between about 1.9 and 3.5 microns, a very small part of the incident energy will be in the cell's "visible" spectrum for the lower temperatures. However, as the black body temperature is increased, a greater portion of the incident power will lie in the detectable wave length range, resulting in a greater response for the same total power input. For the proposed application in which an interference filter is used, all the energy in the selected operating bandwidth lies within the region of maximum response of the detector and hence all filtered incident

radiation will be "seen" by the cell. It follows, then, that the cell responsivity should correspond to the maximum temperature line on Fig. 28. The maximum response for the cell closely approximates the 2000-3000°K black body curve, and this will be used for design. The responsivity given by this curve must be corrected for those parameters differing from the standard conditions, for example, the time constant, cell area, and cell resistance. Typical correction curves are shown in Figs. 29 and 30. Evaluating the following expression,

$$R(db) = R_{standard} + \Delta R_{time\ const} + \Delta R_{cell\ area\ resistance}$$

yields a cell responsivity of

$$R(db) \doteq 40 + 15 + 5 = 60 \text{ db/microwatt}$$

which is

$$R = 1000 \text{ volts/watt}$$

For the selected design radiation signal of Fig. 24, a signal level of approximately 100 to 1000 microvolts is predicted for the detector output.

This signal must be amplified and transmitted to the end device. The amplifier should have a bandwidth from 0-50 kilocycles and amplify the microvolt signal to an acceptable level for coaxial cable transmission. An oscilloscope, such as the Tektronix 535, should serve quite satisfactorily as an end device, with the addition of a Land Camera, to record the output trace.

A most critical problem will be the prevention of stray pickup by the transmission leads and by the circuitry within the shock tube

instrument housing. Radiation from the stray electromagnetic fields will be quite extensive. The 25-kilovolt discharge in the shock tube and the intense magnetic field from the nose coil and the associated leads will generate a great deal of this spurious radiation. To shield the oscilloscope, it will be placed in a copper screen room about 20 feet from the shock tube. The detector-amplifier unit will be enclosed in the copper housing which leaves only the coaxial cable lead from the housing as a source of stray pickup. The use of a differential amplifier at the oscilloscope will minimize the effect of this stray pickup. Elementary tests should be conducted to determine whether or not additional shielding is required.

The amplifier unit should have a high input impedance matching the detector cell resistance. An amplifier gain of approximately 1500 should be ample. Power supply space is extremely critical and the undesirability of operating the amplifier with a remote supply, due to stray pickup, suggests the use of transistors. The direct-coupled amplifier design in Fig. 31 with a grounded collector input stage should prove to be adequate.

7. Calibration.

The analysis of the preceding sections suggests that the magnitude accuracy of the measured heat transfer rate will be somewhat in doubt. The transmission path attenuation values, expected cell and interference filter performance and many other factors were estimated as closely as possible, but to measure the heat transfer rate quantitatively, it becomes necessary to devise a means of calibrating the system. The most obvious method is to subject the film to an electrical energy input that dynamically simulates the heat energy input of the shock tube tests, and record the detection system response. The joule heating of the gold film will simulate the heat flux and it should be possible to record various readings for various magnitudes and durations of current pulses through the film. The peak current required for the 5000 Å thick gold film appears excessive for usual methods of current pulsing, due to the low resistance offered by the film. Extrapolating the findings of Holland, [24] it is expected that for film thicknesses somewhat greater than 1000 Å, the bulk resistivity for gold is valid. From the resistance relationship,

$$R = \rho \frac{\ell}{A} \text{ ohms}$$

and assuming a square film, 0.38 centimeter on a side, the resistance is found to be approximately 5×10^{-2} ohms.

Simulating a heat transfer rate of 5000 Btu/sec-ft^2 would require 650 watts of power or about 115 amperes discharged through the film for the desired time interval. The difficulty in controlling this magnitude of current gives rise to the undesirable, but perhaps necessary, alternative of calibrating the system with a thinner film, and then replacing the 5000 Å film for measurements. High currents of long

time duration would very likely physically destroy the film, or arc over at the contacts, preventing dissipation of the desired energy input. Hot spots would probably disturb the homogeneity of the film surface and destroy the infrared opacity. Based on values reported by Holland, a 100 Å thick gold film will have a resistance of approximately 40 ohms. Calibrating with this film will permit dynamic heating of a foil to the expected experimental temperatures with a current of about three to four amperes. The radiation given off by the 100 Å film should closely approximate that energy emitted by the 5000 Å film. Interchanging the film-substrate configuration for calibration purposes will undoubtedly lead to a variation in transmission path efficiency, due to physical differences in the interfaces between the gold film and the substrate, and between the substrate and the sapphire light tube. Also the physical properties of the quartz substrates may not be identical.

However, a calibration would seem of interest even if the accuracy is only within 50 per cent of the true value. The 100 Å film can be pulsed for a desired time interval with various current magnitudes corresponding to different heat transfer rates. Equating the joule heating rate to the heat transfer rate,

$$I^2 R = qA$$

the magnitude of the current pulse in terms of time and heat transfer rate can be determined by

$$I(q, t) = \sqrt{\frac{qA}{R(q, t)}} \text{ amperes}$$

where

$$R = R_o(1 + \alpha \Delta T)$$

α = thermal coefficient of resistivity

It is desired to express the change in temperature in the expression above as a function of time. For very thin films, as shown in Sect. 3 and elsewhere, [25] the temperature change of the film can be expressed as,

$$\theta(x, t) = \Delta T(x, t) = \frac{2q}{\sqrt{\pi c_p \rho k}} \sqrt{t} \quad \text{for} \quad x = 0$$

where the physical properties are those of quartz.

$$\Delta T(0, t) = 8.5\, q \sqrt{t}\ (^\circ K)$$

then

$$I(q, t) = \sqrt{\frac{q A_f}{R_o}}\, (1 + 8.5\, \alpha q \sqrt{t})^{-1/2} \text{ amperes}$$

Assuming the bulk value for the thermal coefficient of resistivity is valid, the current pulses corresponding to different heat transfer rates for a film resistance of 100 ohms are plotted in Fig. 32. This indicates that a current supply network capable of one to five ampere pulses, with a duration of 15 to 40 microseconds, should prove adequate for heat transfer rates of interest. Average current values will be used here approximating the actual curves of Fig. 32.

In order to handle the magnitude of currents required in the desired time duration, the use of electronic switching is suggested. Thyratrons with the required current carrying capacity such as type 3D22A can be utilized as switches. In order to supply this

current, conventional power supplies of milliampere capacity will not suffice. It seems logical to store the required charge on a high voltage capacitor. The circuit shown in Fig. 33 was suggested by the authors and appears to meet the requirements. The two thyratrons are normally off, with the control grids held negative by the grid bias. The capacitor, C_c, is charged to the desired plate voltage, with the switch in position No. 1. When the capacitor has been charged, the switch is shifted to position No. 2, the desired current magnitude set up by means of the potentiometer, R_p, and the pulse duration, Δt, selected on the pulse generator and delay network. When the pulse generator is triggered, pulse No. 1 turns thyratron No. 1 on, permitting current to flow through the gold film. Pulse No. 2 turns thyratron No. 2 on after the desired pulse duration, and shorts the potentiometer and gold film to ground.

However, experimental determination of the conductivity characteristics of the 100 Å thick film should be made prior to actually pulsing the film. The conductivity of the film should be investigated over the temperature range of interest, and the values obtained used to determine current pulse characteristics such as those shown in Fig. 32. When this has been accomplished, then the actual calibration can take place, utilizing the described network.

Other means of calibration that could be investigated are:

(1) Heating a film on a separate substrate, and then placing the configuration in contact with the sapphire rod

(2) Alternating current joule heating

(3) Ignitron current pulsing.

Suggestions 1 and 2 are static methods, but would seem simple to perform, and could give quite accurate calibration for known film temperatures. A thermocouple could be utilized to provide precise film temperature measurements at the time of calibration.

Method 3 offers the hope of dynamic calibration of the 5000 Å film with electronic control. However, as stated previously, whether or not the film can physically withstand current pulses of the required magnitude remains to be determined.

8. Conclusions.

It is concluded from this analysis that the proposed infrared system will be capable of measuring stagnation point heat transfer rates on test bodies subjected to simulated space flight conditions in an electromagnetic shock tube. The ultimate design consists of a thin metallic film evaporated on a quartz window. Radiation through the quartz window is transmitted via a sapphire light pipe to a sensitive lead sulphide detector cell. The output of the cell is amplified and observed on a conventional oscilloscope.

It was found that optimum system performance will be achieved by

(1) Use of a gold film evaporated on a fused quartz substrate

(2) A film thickness of 5000 $\mathring{A}$

(3) A sapphire light pipe as a most efficient means of energy transmission in the near infrared spectrum

(4) Selection of a lead sulphide cell

(5) Choosing a spectral bandwidth of 0.4 micron centered at a wave length of approximately 2.8 microns

(6) An interference filter to limit the lower wave length energy striking the detector cell

(7) Electromagnetic shielding of all electrical circuitry.

The apparatus will be useable under the ionized flow conditions in which present resistance film gages are inoperative. It is believed that heat transfer rates of approximately 2000 to 35,000 Btu/ft^2-sec can be measured within the 15 to 40 microsecond observation periods. The upper value is limited by the melting temperature of the gold film or the detector cell time constant. The lower limit is the minimum

heat transfer rate which will produce a detectable film temperature within the maximum available test time.

The accuracy of the absolute heat transfer rate measurement will be somewhat doubtful, until a more appropriate means of calibration is devised. The proposed method should suffice for preliminary experimentation and relative measurements, but more precise calibration of the apparatus will be of future value. Further calibration studies should be undertaken to achieve the ultimate system capability.

Investigation of the following subjects of current interest could be undertaken with this apparatus.

(1) Radiative, convective, and recombination heat transfer to bodies in hypersonic flow

(2) Effect of magnetic fields on radiative, convective, and recombination heat transfer rates.

The system will be assembled and ready for experimental work during the summer of 1959. Experimental difficulties remain to be found and remedied, but it is believed no major problem should arise. The first application of the apparatus will be to verify the theoretical work done in magnetoaerodynamic cooling. The successful completion of this experimental work should greatly contribute to future space vehicle design and performance.

9. References.

1. R. C. Meyer, On Reducing Aerodynamic Heat Transfer Rates by Magnetohydrodynamic Techniques, Preprint No. 816, Institute of the Aeronautical Sciences, January, 1958.

2. W. B. Bush, Unpublished Note on Magnetohydrodynamic-Hypersonic Flow Past a Blunt Body, Space Technology Laboratories, Note PRL-9-07, February 4, 1959.

3. R. W. Ziemer and W. B. Bush, Magnetic Field Effects on Bow Shock Stand-off Distance, Physical Review Letters, vol. 1, no. 2, July 15, 1958.

4. R. J. Vidal, Model Instrumentation Techniques for Heat Transfer and Force Measurements in a Hypersonic Shock Tunnel, Report AD-917-A-1, Cornell Aeronautical Laboratory, Inc., Buffalo, New York, February, 1956.

5. F. S. Harris, Jr., Measurement of Temperature in Explosives, Explosives Research Group, University of Utah, Salt Lake City, Utah, August, 1953.

6. E. B. Mayfield, Four-Color Radiometric Temperature of Hypervelocity Projectiles, paper presented at 1958 Summer Meeting in the West of the American Physical Society at Vancouver, British Columbia, August, 1958.

7. Infratron Lead Sulphide Photoconductors, Brochure, Infrared Industries, Inc., Waltham, Massachusetts, September, 1958.

8. T. Wentink, Jr., W. Planet, P. Hammerling, and B. Kivel, Infrared Continuum Radiation from High-Temperature Air, Journal of Applied Physics, vol. 29, April, 1958.

9. R. W. Ziemer, An Electromagnetic Shock Tube for Aerodynamic Research, Space Technology Laboratories, Report GM-TR-0127-00419, June, 1958.

10. E. B. Turner, Description of the Revolving Mirror Streak Camera Built by the Aeronautical Research Laboratory, The Ramo-Wooldridge Corporation, Report ARL-7-40, September, 1957.

11. F. R. Gilmore, Equilibrium Composition and Thermodynamic Properties of Air to 24,000°K, Rand Corporation, Report RM-1543, August, 1955.

12. R. W. Detra, N. H. Kemp, and F. R. Riddell, Addendum to Heat Transfer to Satellite Vehicles Re-entering the Atmosphere, Jet Propulsion, vol. 27, no. 11, December, 1957.

13. R. E. Meyerott, Radiation Heat Transfer to Hypersonic Vehicles, Lockheed Aircraft Corporation, Missile Systems Division, Report LMSD-2264-R1, September, 1958.

14. O. S. Heavens, Optical Properties of Thin Solid Films, p. 55, Academic Press, Inc., New York, New York, 1955.

15. Fused Quartz Catalog, No. Q6, General Electric Company, 1957.

16. R. V. Churchill, Modern Operational Mathematics in Engineering, McGraw-Hill Book Company, 1944.

17. P. H. Rose, Development of the Calorimeter Heat Transfer Gage for Use in Shock Tubes, Avco Research Laboratory, RR-17, pp. 34-37.

18. A. Erdelyi, W. Magnus, F. Oberhettinger and F. G. Tricomi, Table of Integral Transforms, vol. I, p. 246, McGraw Hill Book Company, Inc., New York, New York, 1954.

19. Rose, pp. 38-41.

20. Sapphire Rod as a Radiation Pipe, Linde Air Products Company, Bulletin No. 4, New York, New York, January, 1957.

21. P. J. Klass, Infrared Revival Challenges Radar, Aviation Week, Reprint, McGraw-Hill Publishing Company, Inc., 1957.

22. R. C. Jones, Performance of Detectors for Visible and Infrared Radiation, Advances in Electronics, vol. V, pp. 67-68, Academic Press, Inc., New York, New York.

23. E. A. Guillemin, Communication Networks, vol. II, p. 468, John Wiley and Sons, Inc., New York, New York, 1935.

24. L. Holland, Vacuum Deposition of Thin Films, pp. 232-239, John Wiley and Sons, Inc., New York, New York, 1956.

25. J. Rabinowicz, M. E. Jessey and C. A. Bartsch, Resistance Thermometer for Heat Transfer Measurement in a Shock Tube, GALCIT, Memo. 33, July 2, 1956.

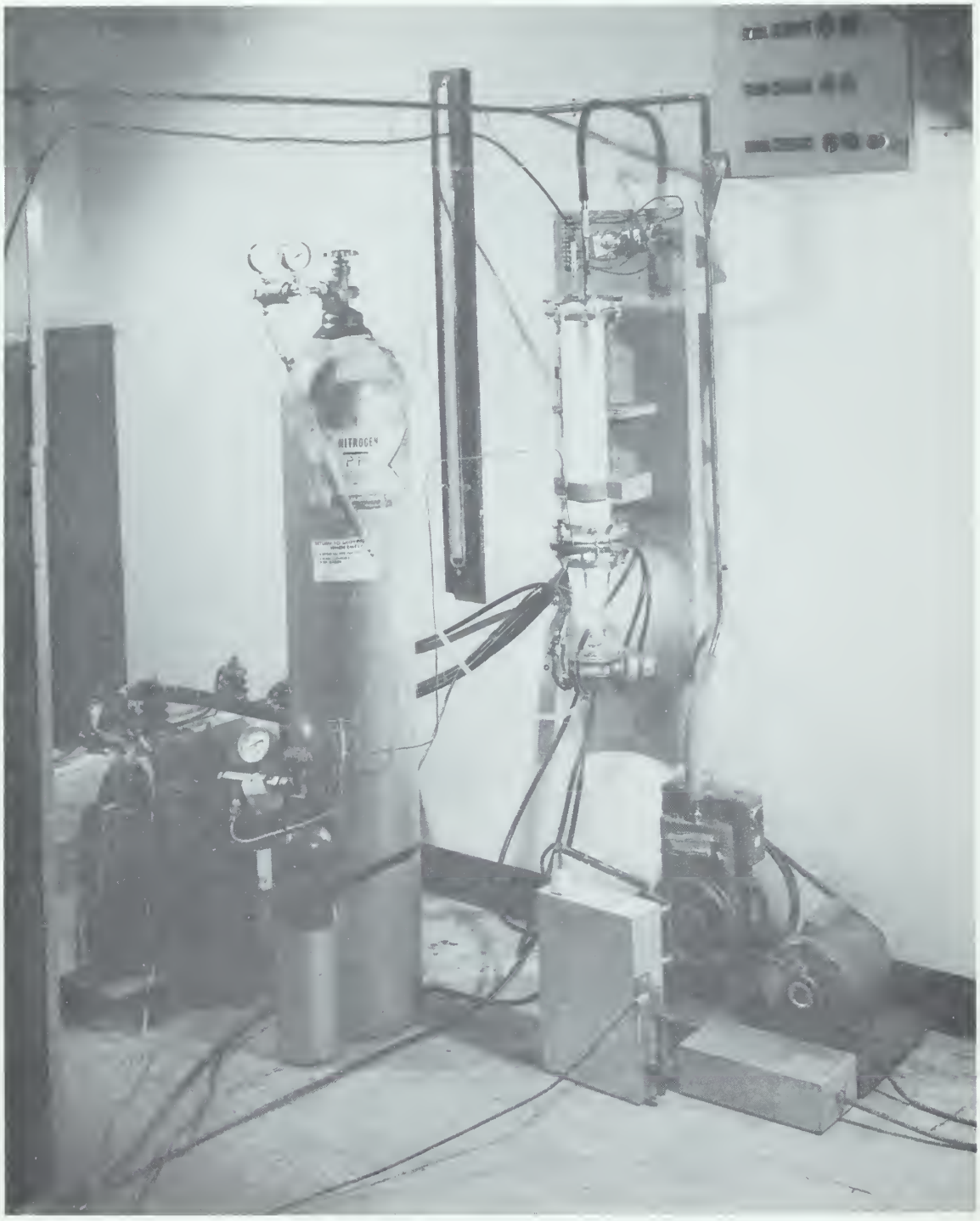

Figure 1. An Electromagnetic Shock Tube in Operation.

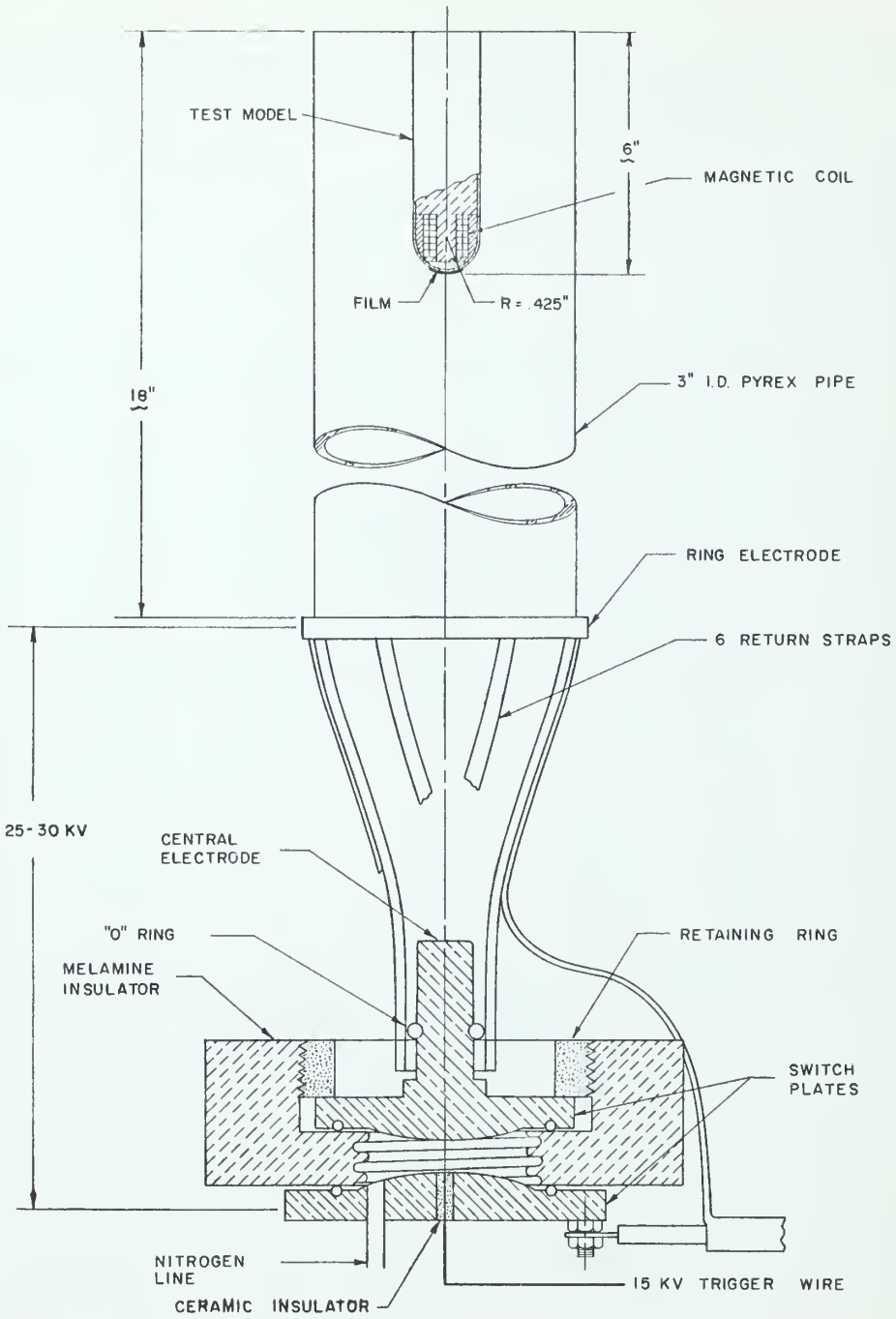

Figure 2. Details of the Shock Tube with the Test Model Installed.

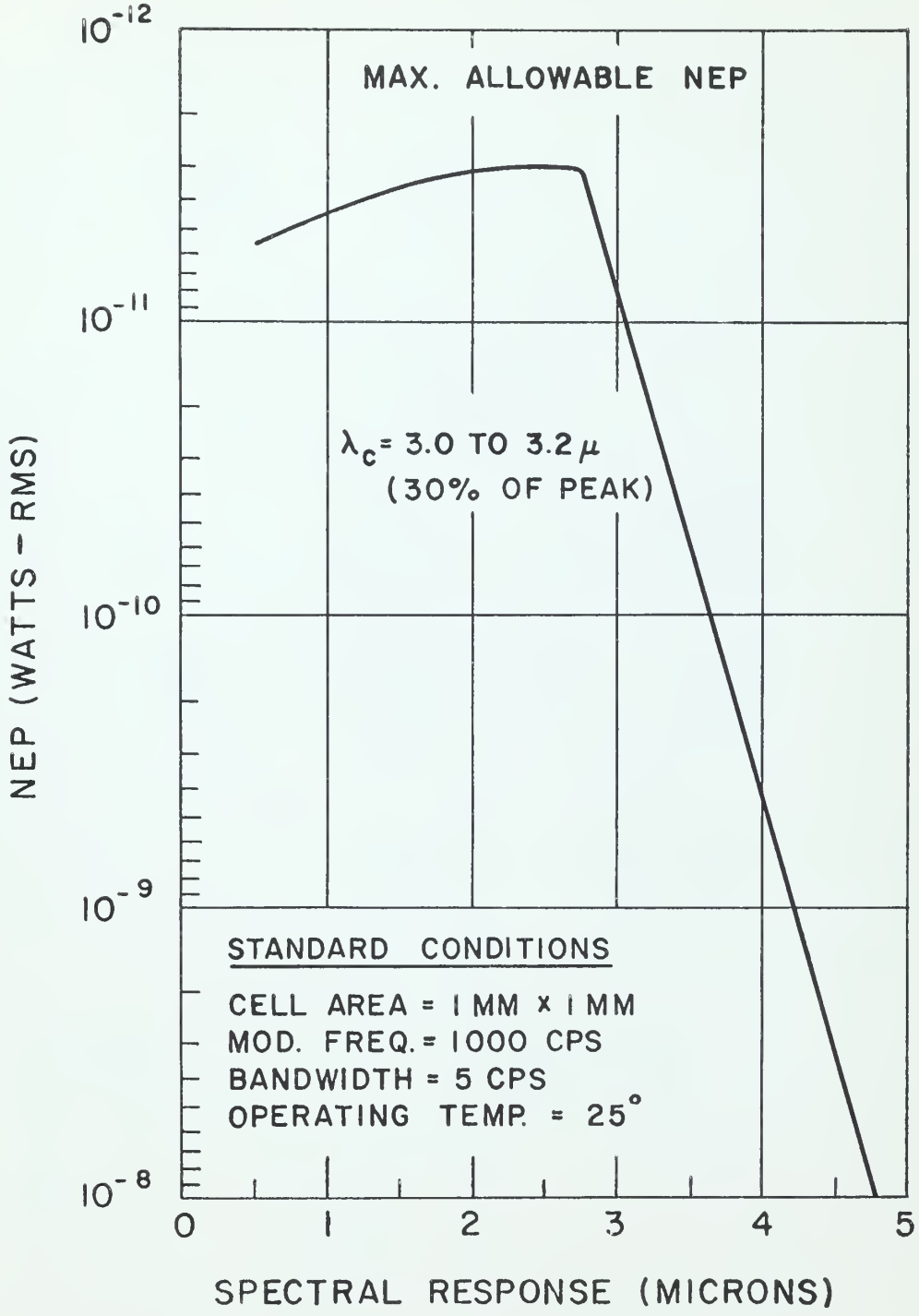

Figure 3. Typical Spectral Response of a Lead Sulphide Cell (noise-equivalent-power).

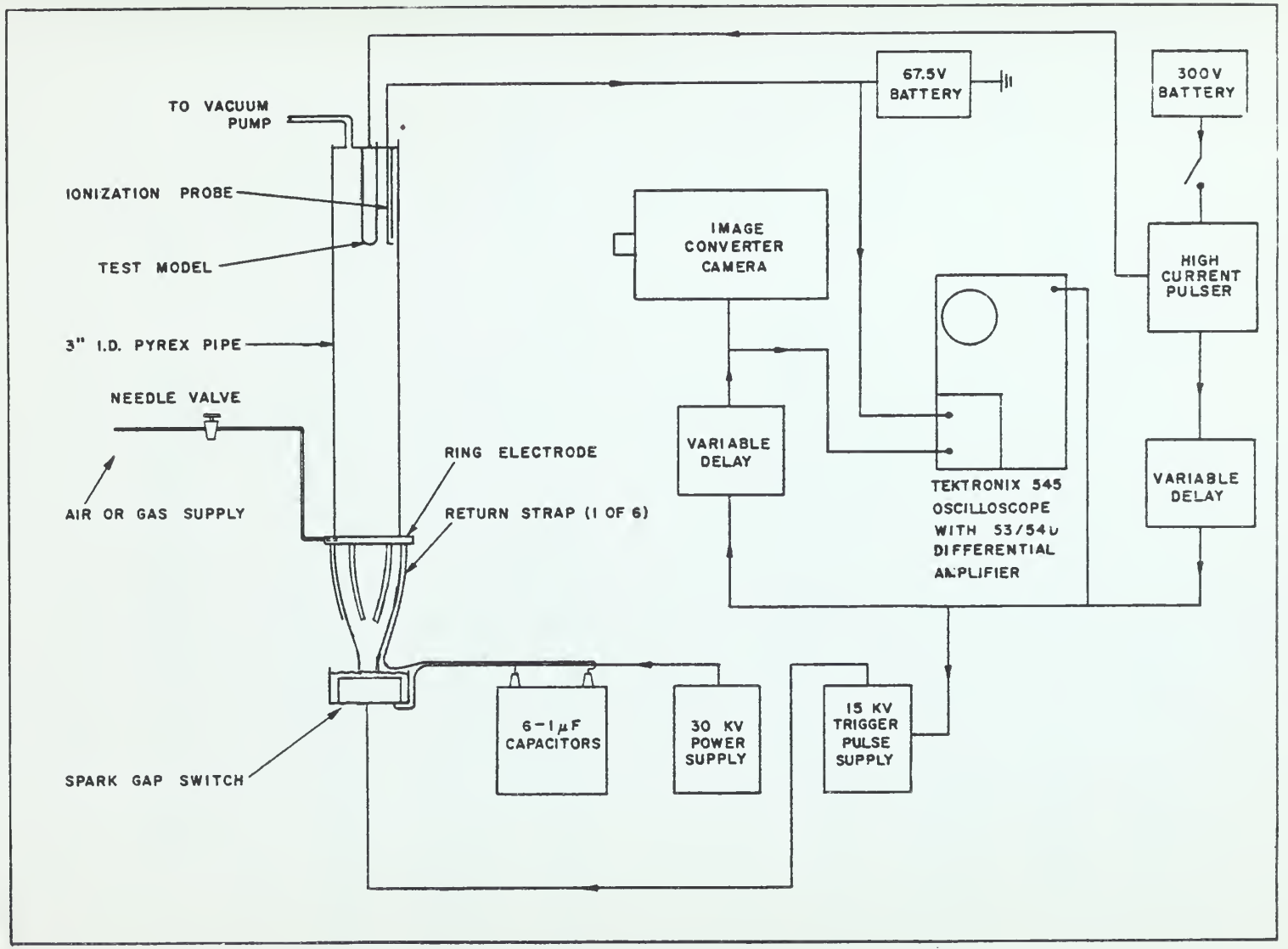

Figure 4. Schematic Diagram of the Shock Tube and Associated Experimental Apparatus.

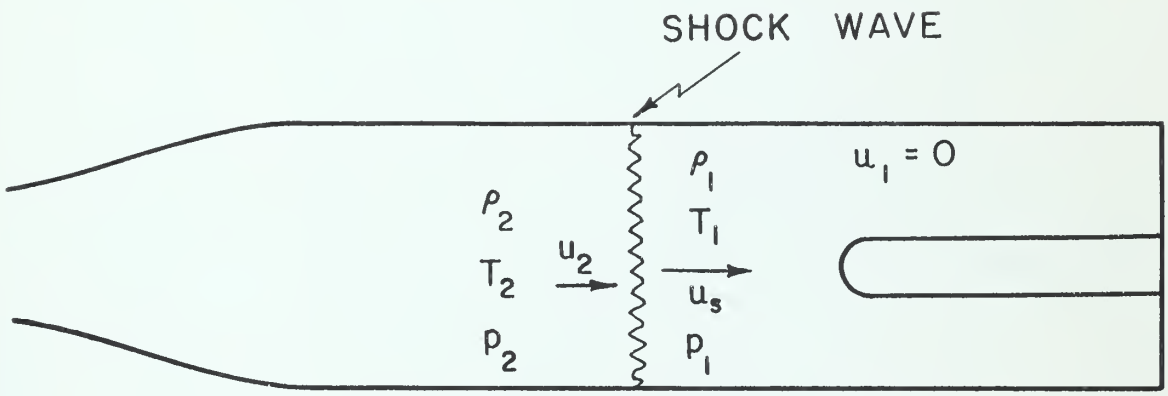

Stationary Model Coordinate System

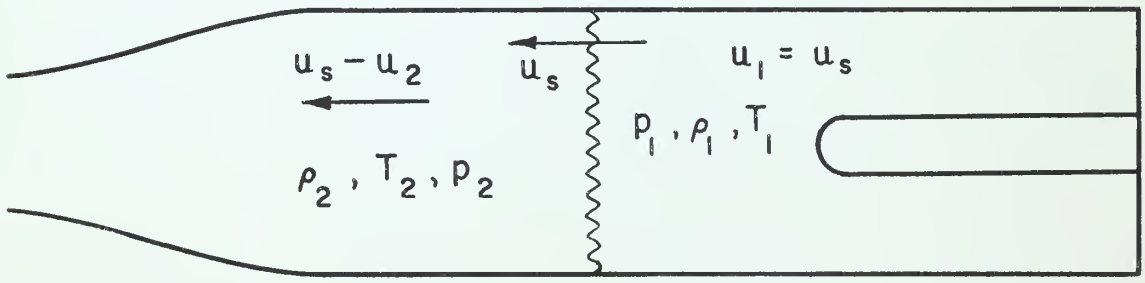

Moving Model Coordinate System

Figure 5. Shock Wave Coordinate Relationships within the Shock Tube.

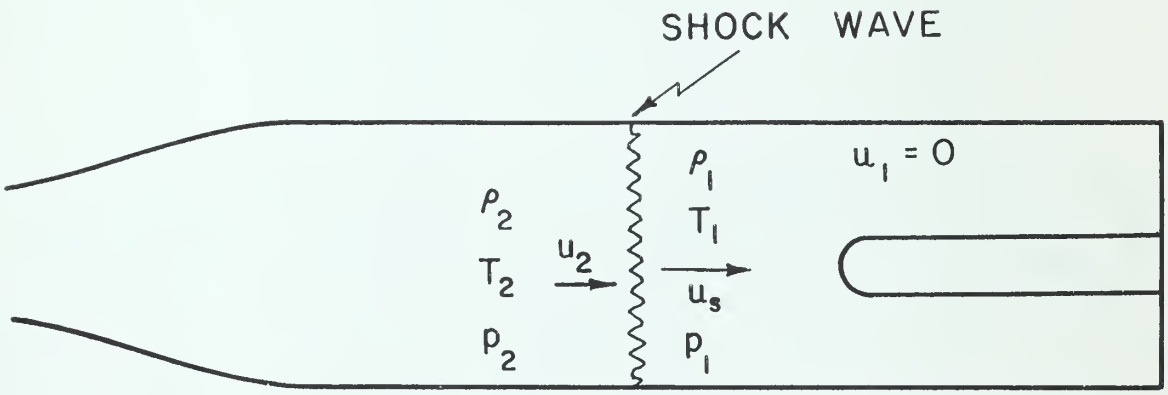

Stationary Model Coordinate System

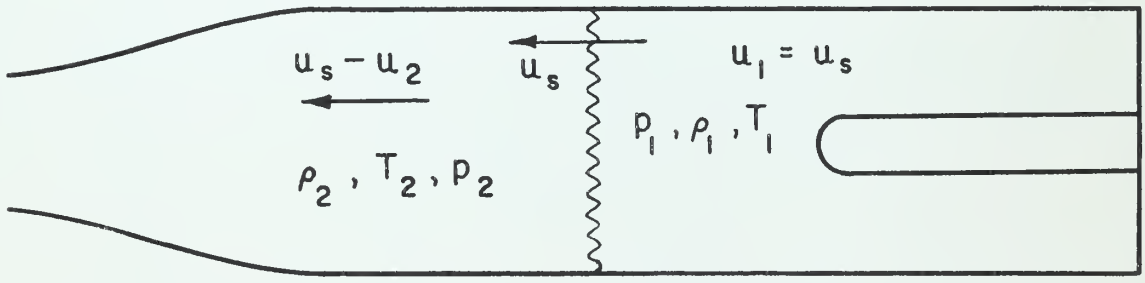

Moving Model Coordinate System

Figure 5. Shock Wave Coordinate Relationships within the Shock Tube.

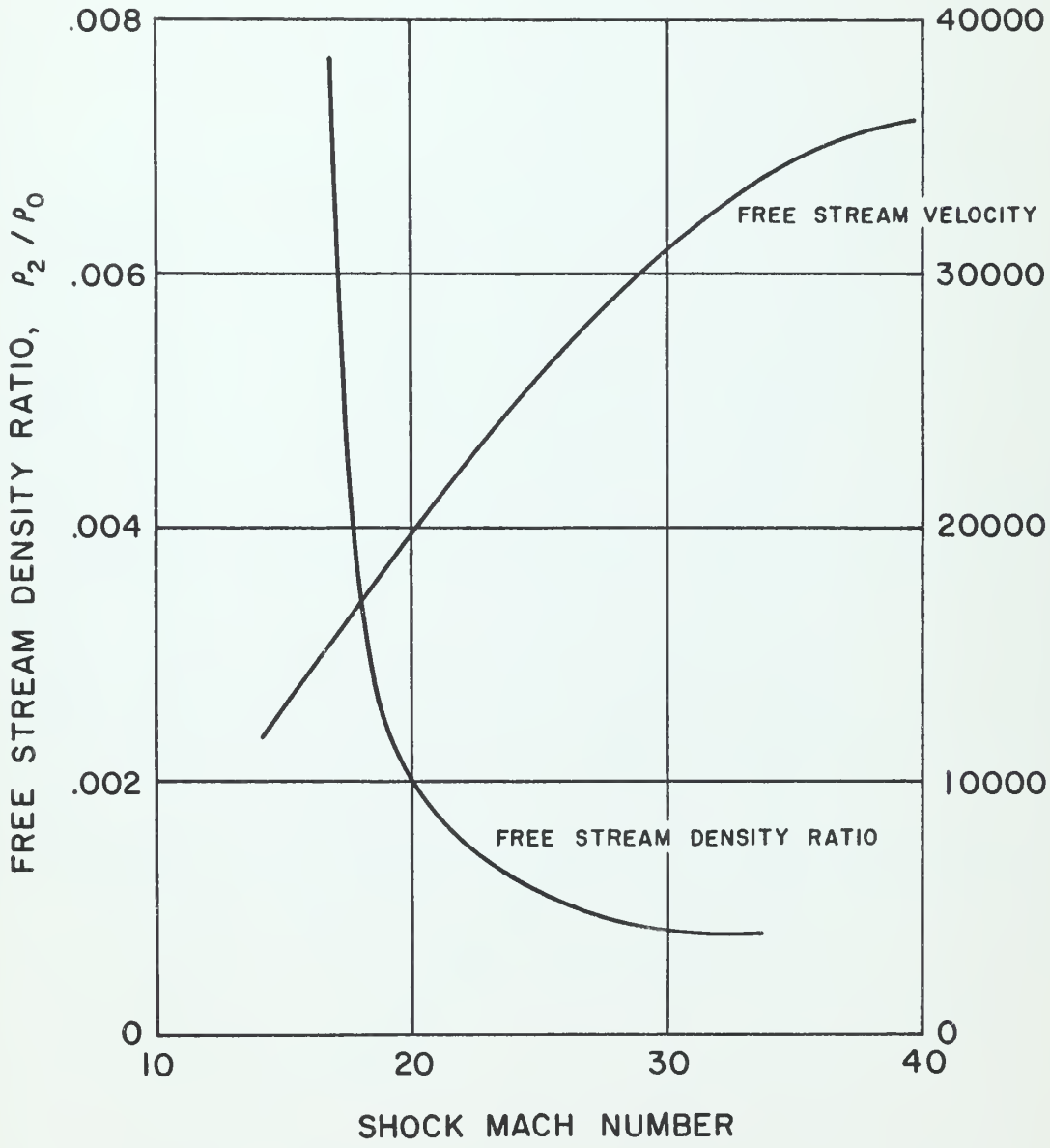

Figure 6. Free Stream Density Ratio and Free Stream Velocity in the Shock Tube.

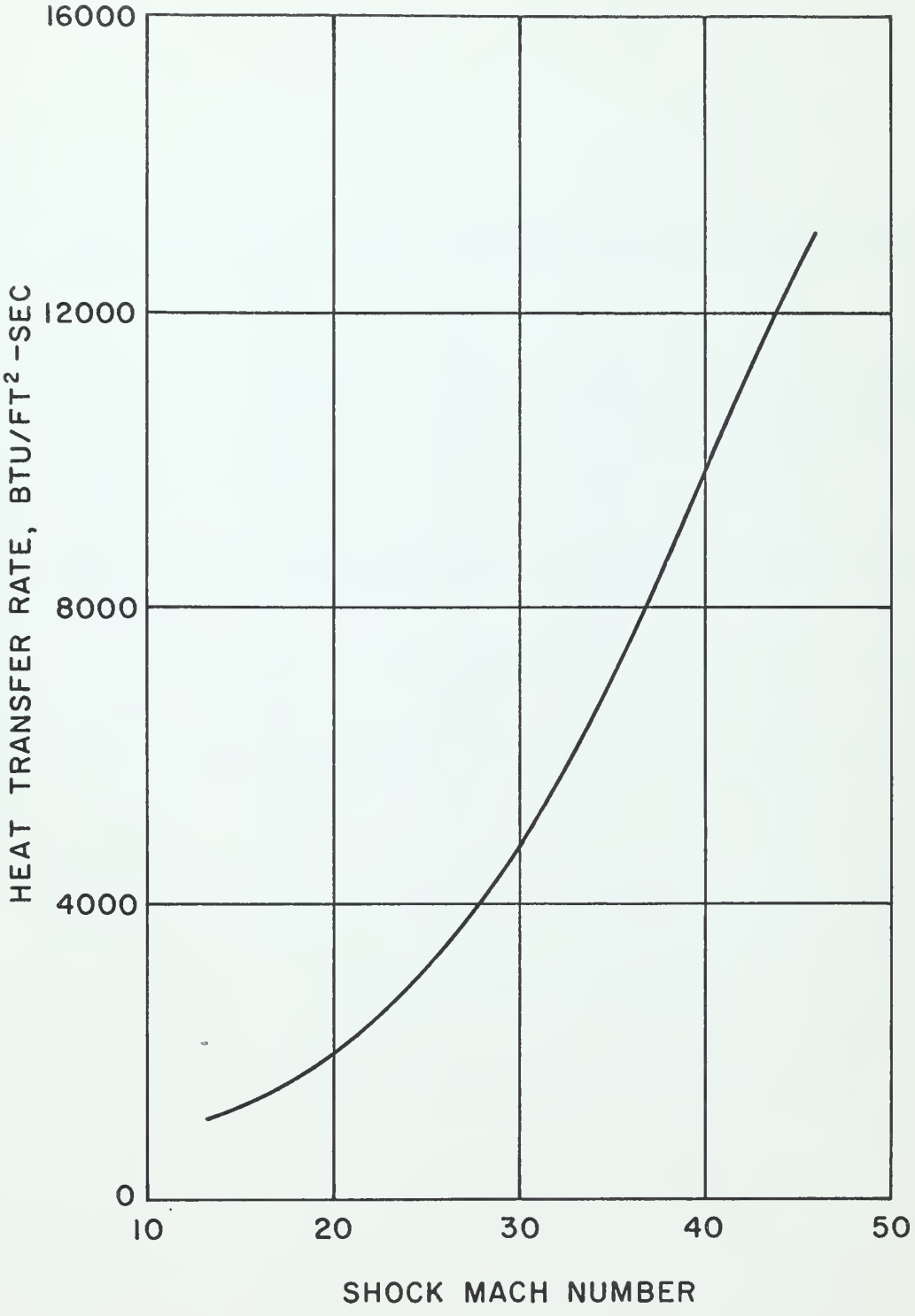

Figure 7. Predicted Heat Transfer Rates.

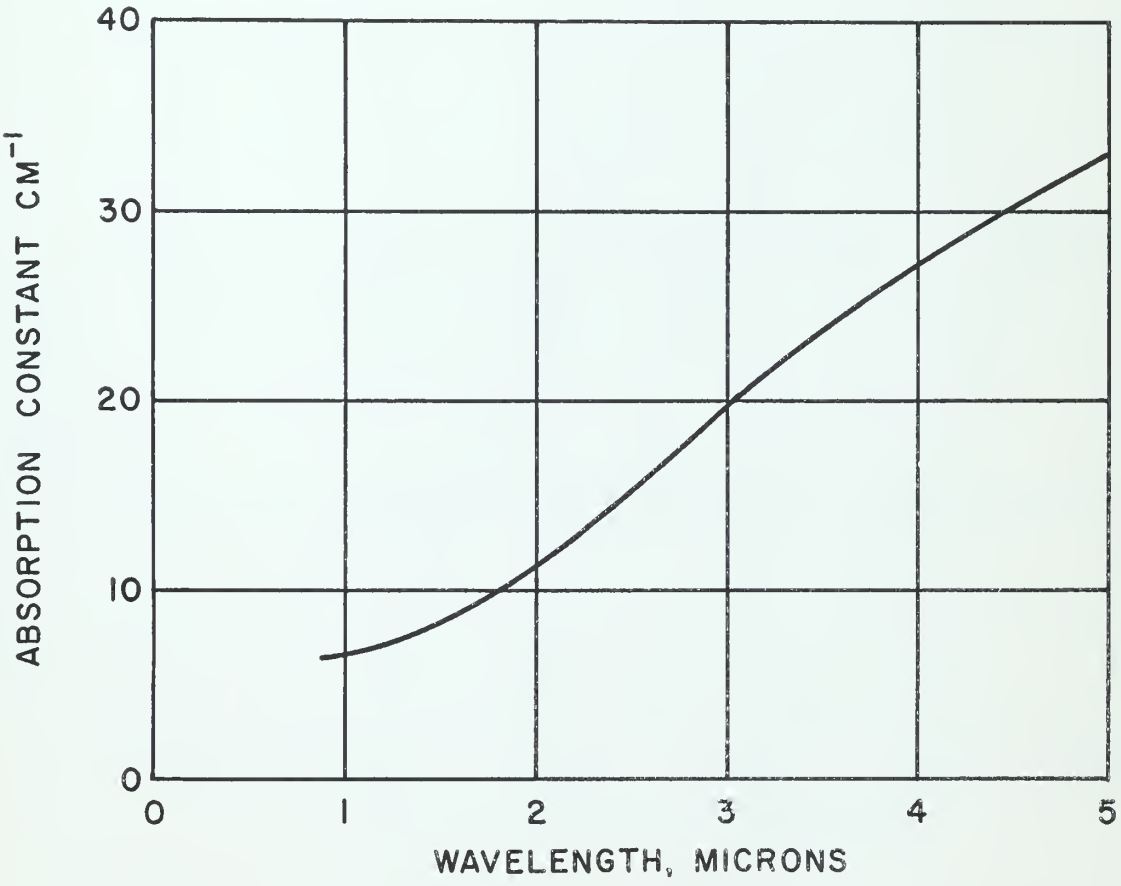

Figure 8. Spectral Absorption Coefficient for Gold.

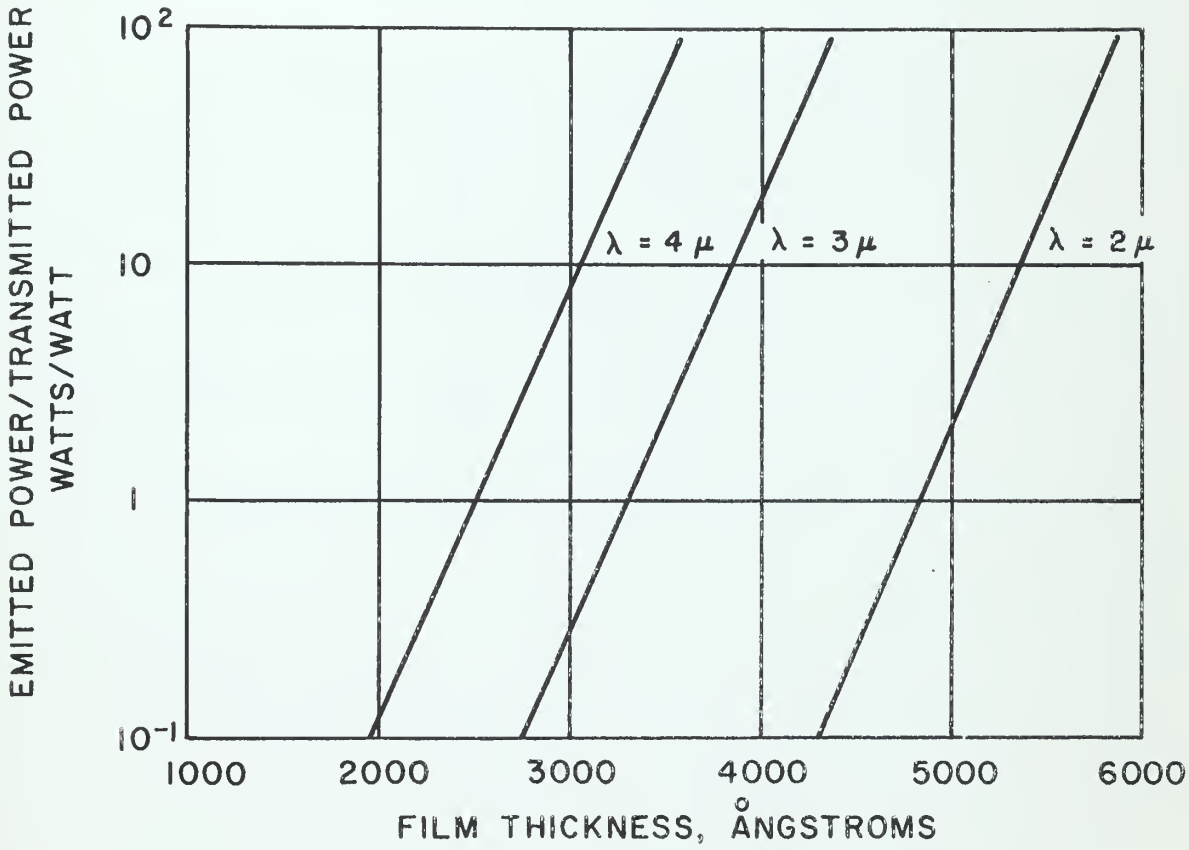

Figure 9. Ratio of Emitted Energy to Transmitted Energy, W_g/W_t, for Various Film Thicknesses.

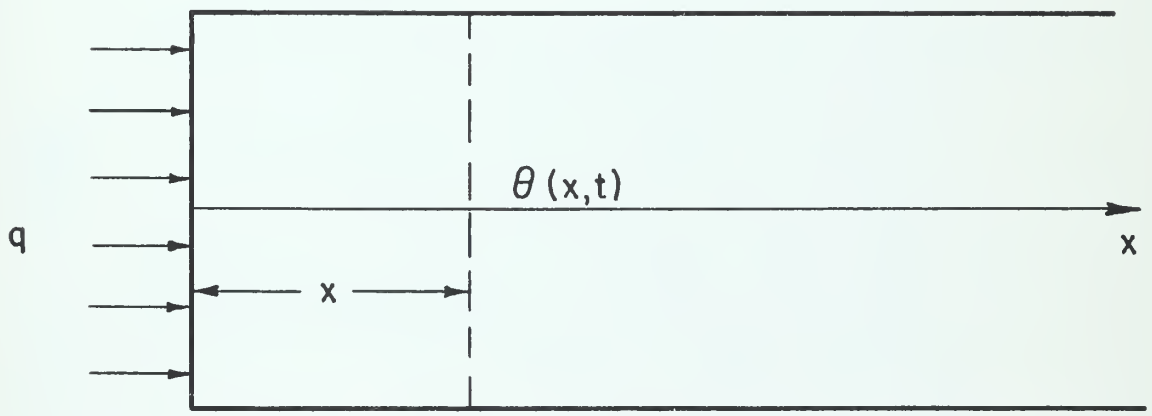

Figure 10. Heat Flow in a Semi-Infinite Slab.

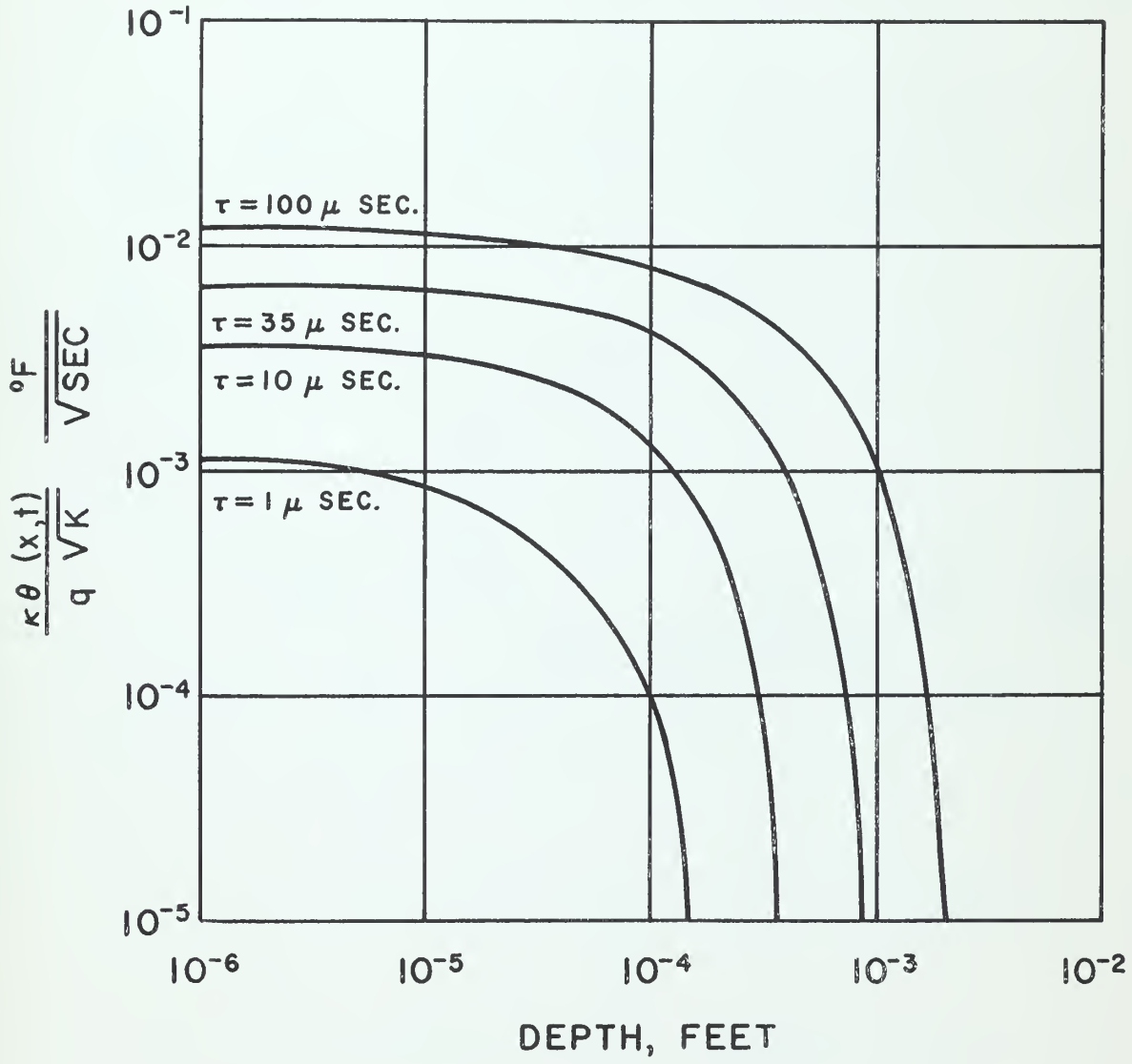

Figure 11. Temperature-Time Profile in a Semi-Infinite Slab.

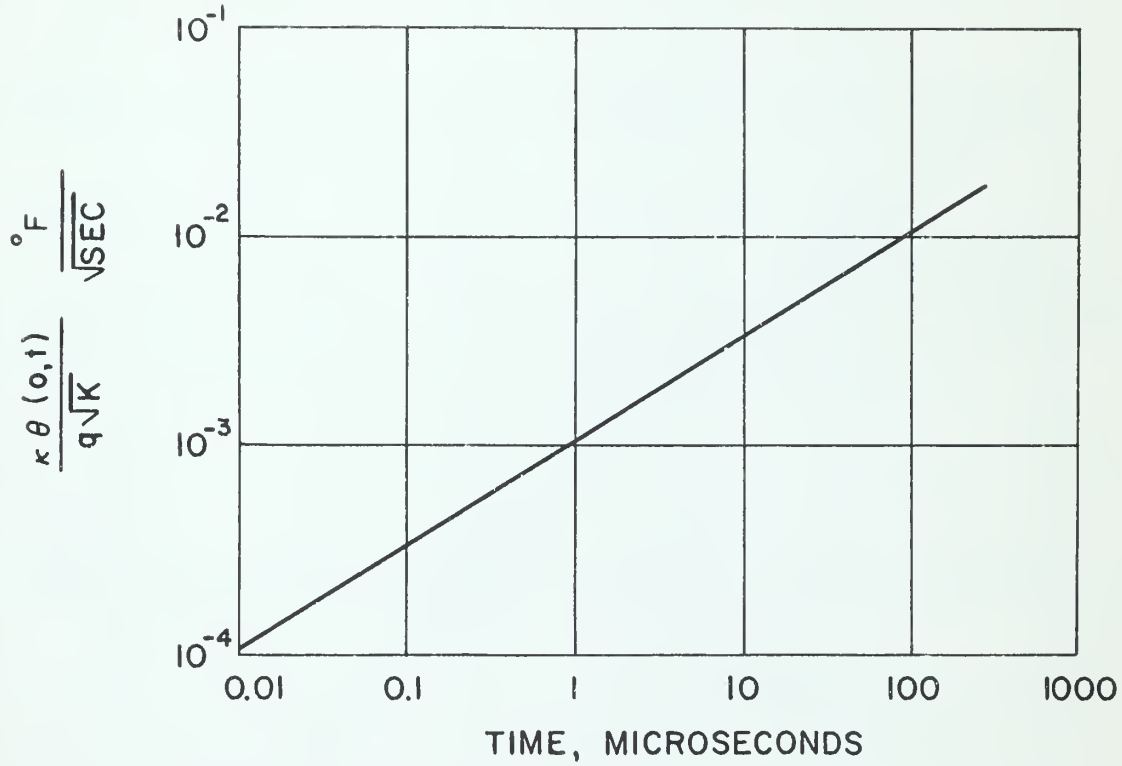

Figure 12. Outer Surface Temperature for a Semi-Infinite Slab as a Function of Time.

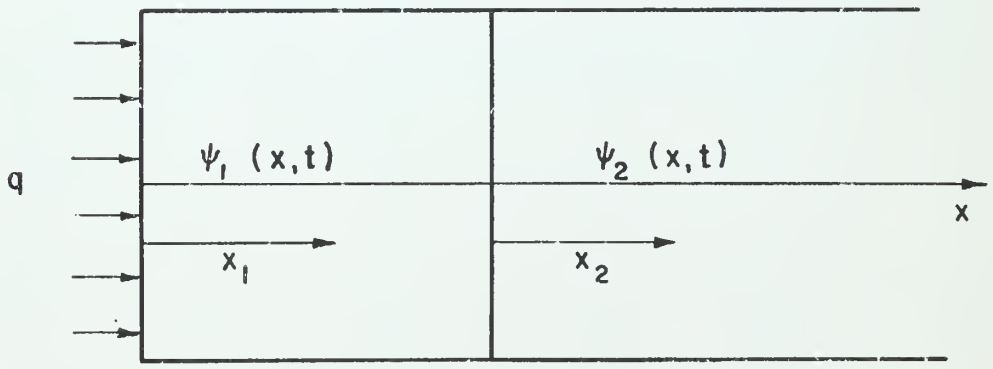

Figure 13. Heat Flow Through a Parallel Wall Slab.

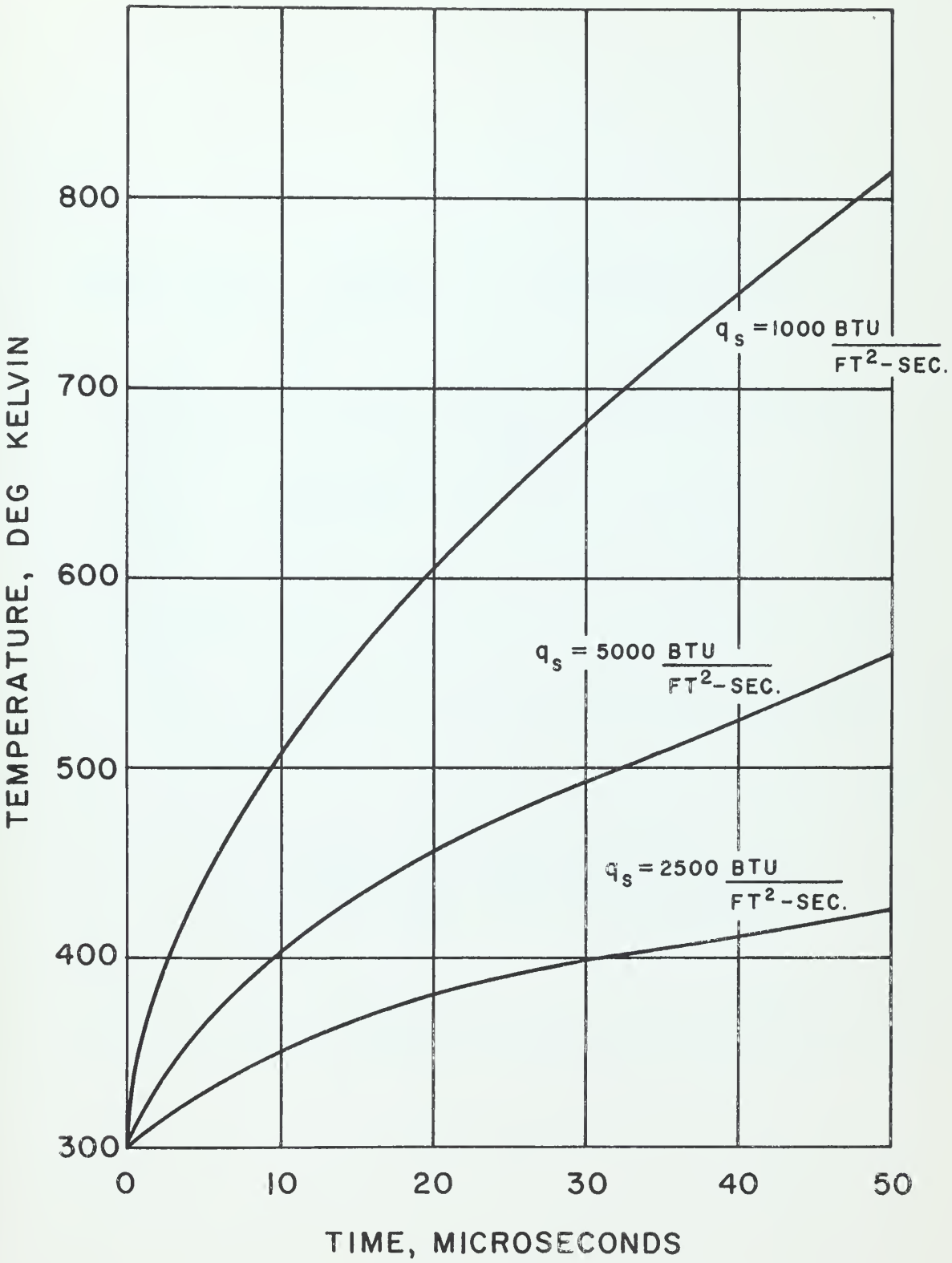

Figure 14. Interface Temperature-Time Relationships.

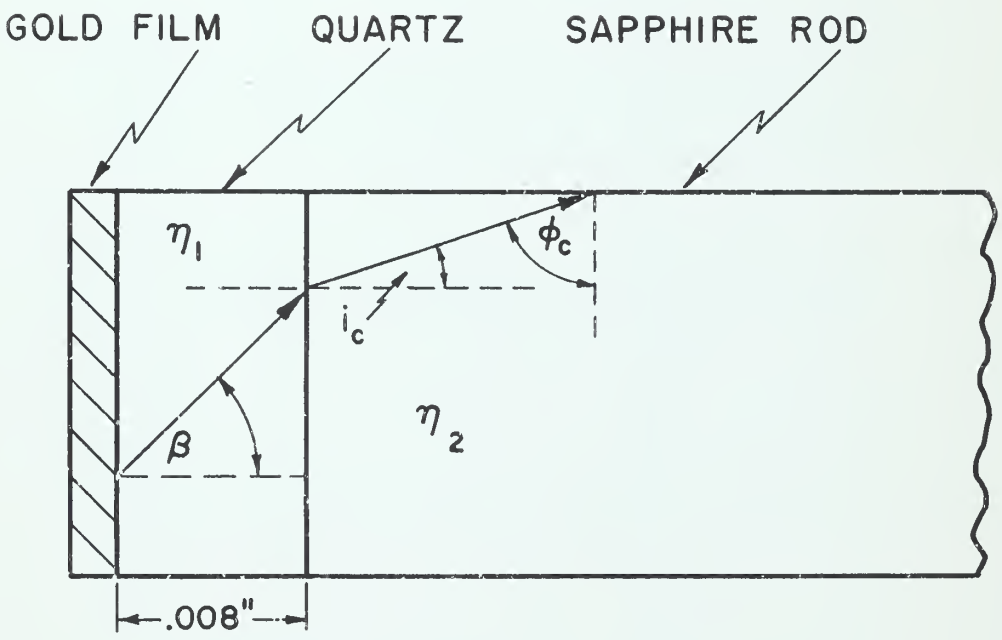

Figure 15. Schematic Diagram of Light Tube Transmission System.

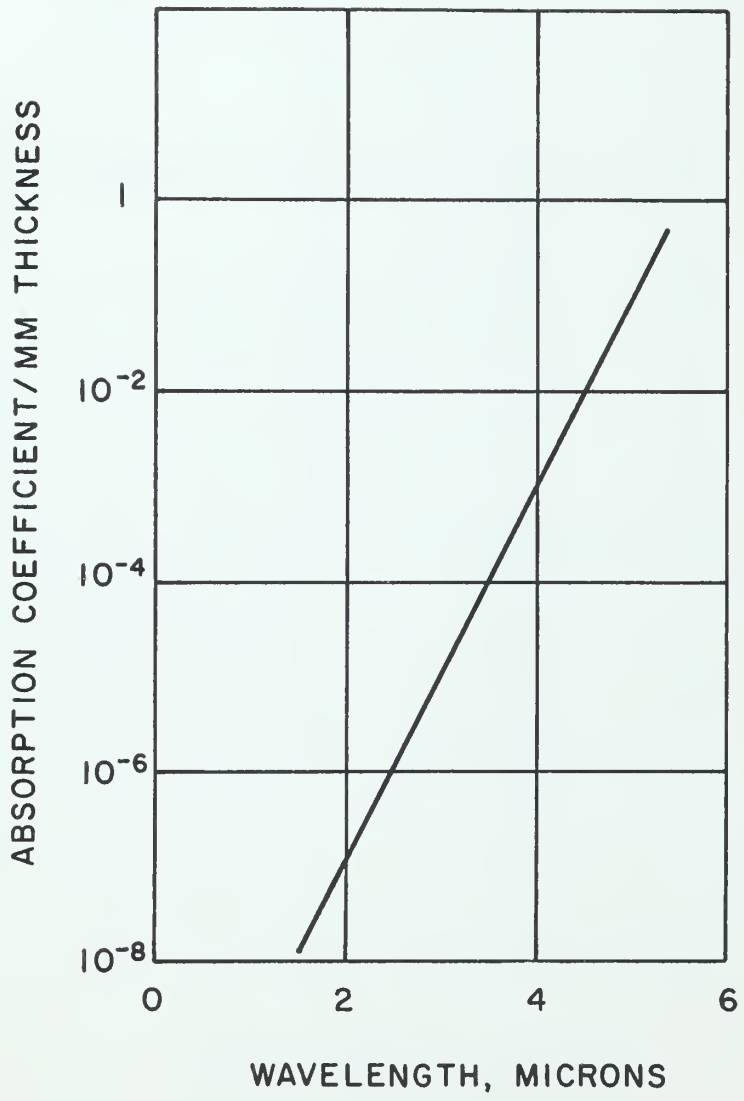

Figure 16. Sapphire Spectral Absorption Coefficient.

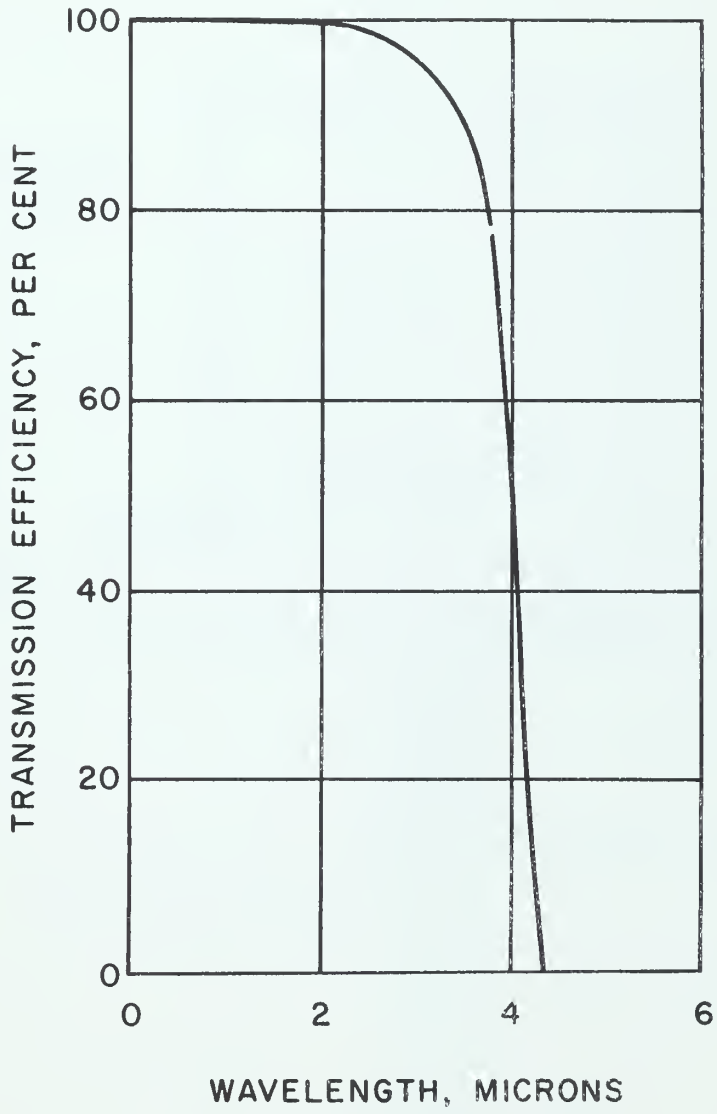

Figure 17. Transmission Efficiency of a Sapphire Light Pipe.

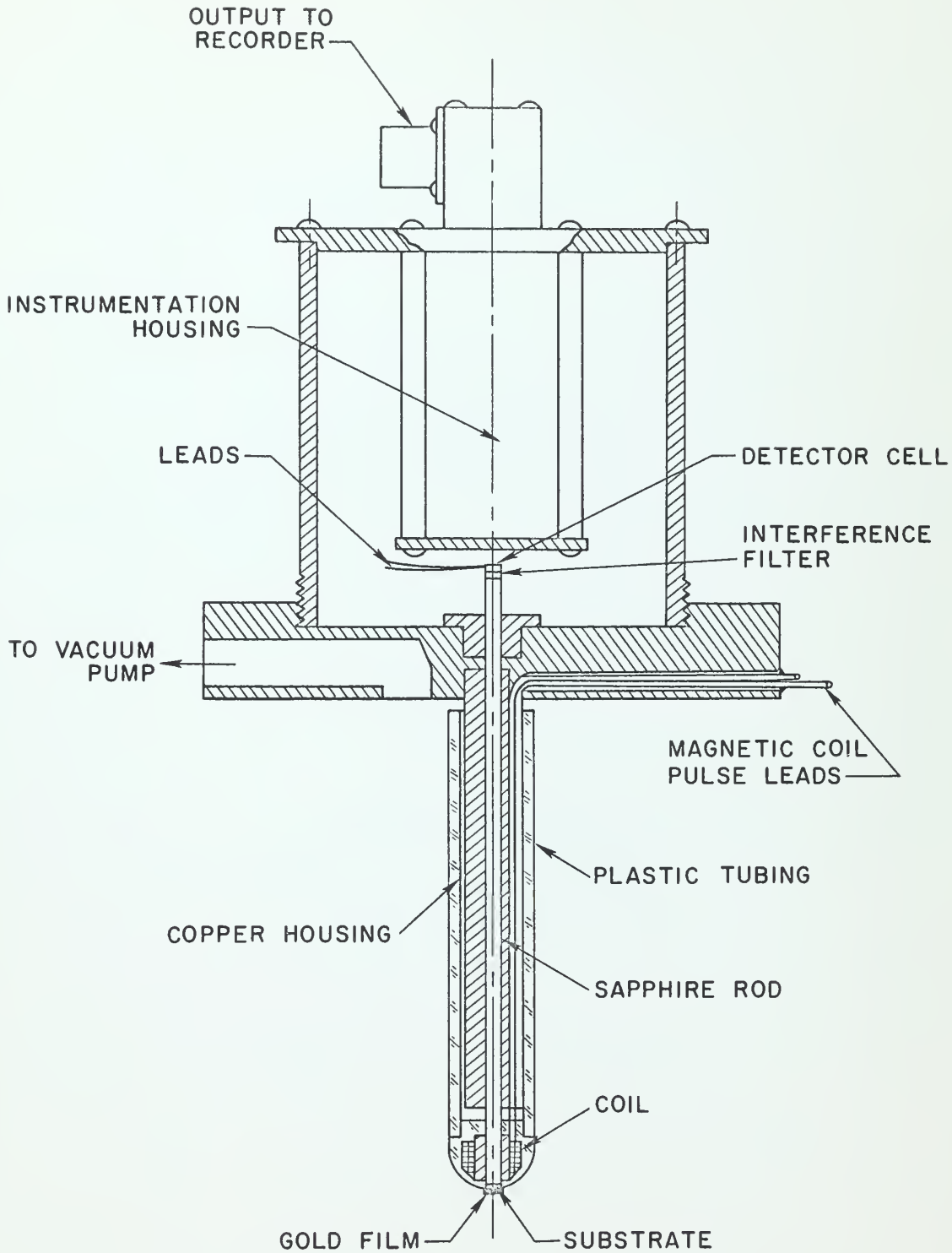

Figure 18. Detailed System Assembly.

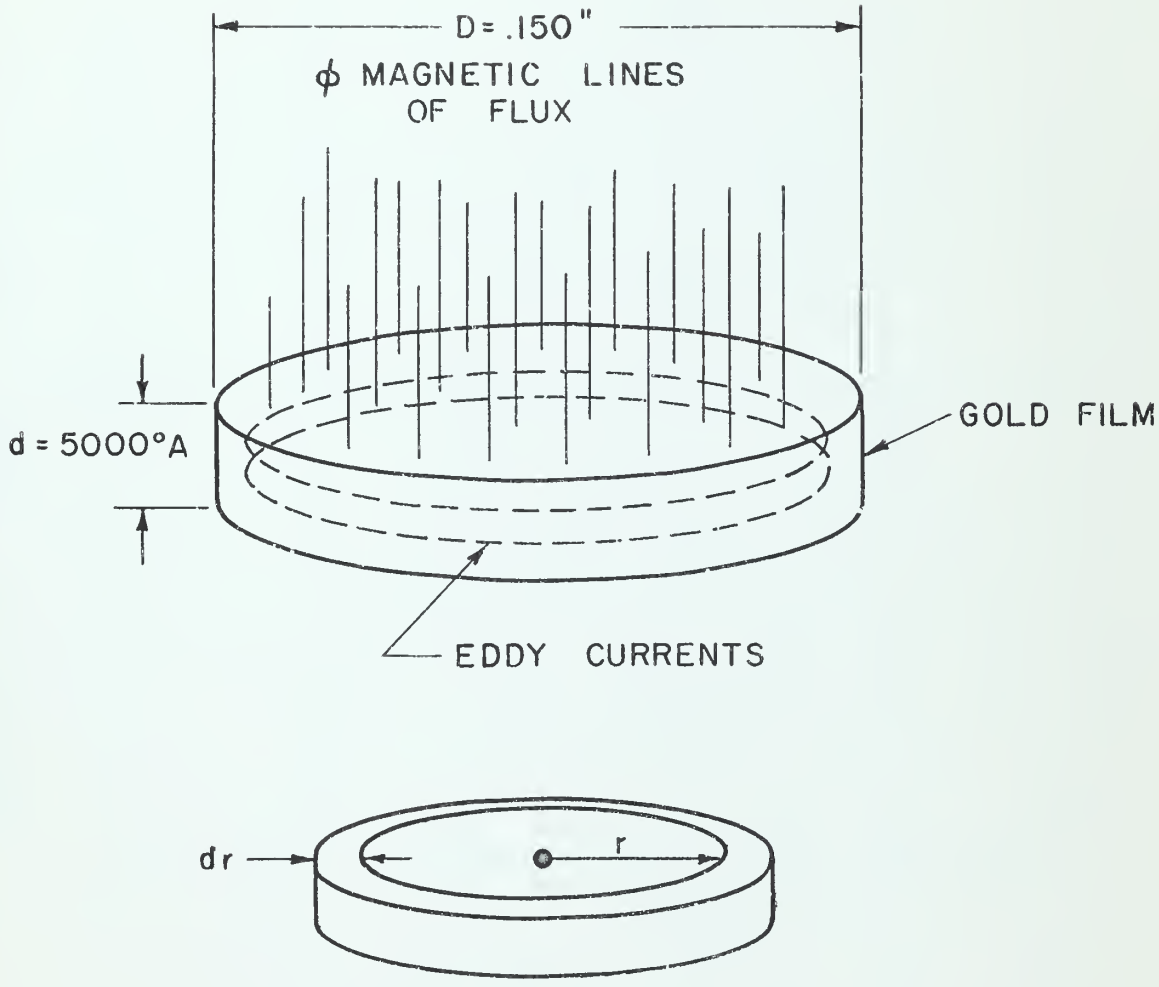

Figure 19. Eddy Current Heating Considerations.

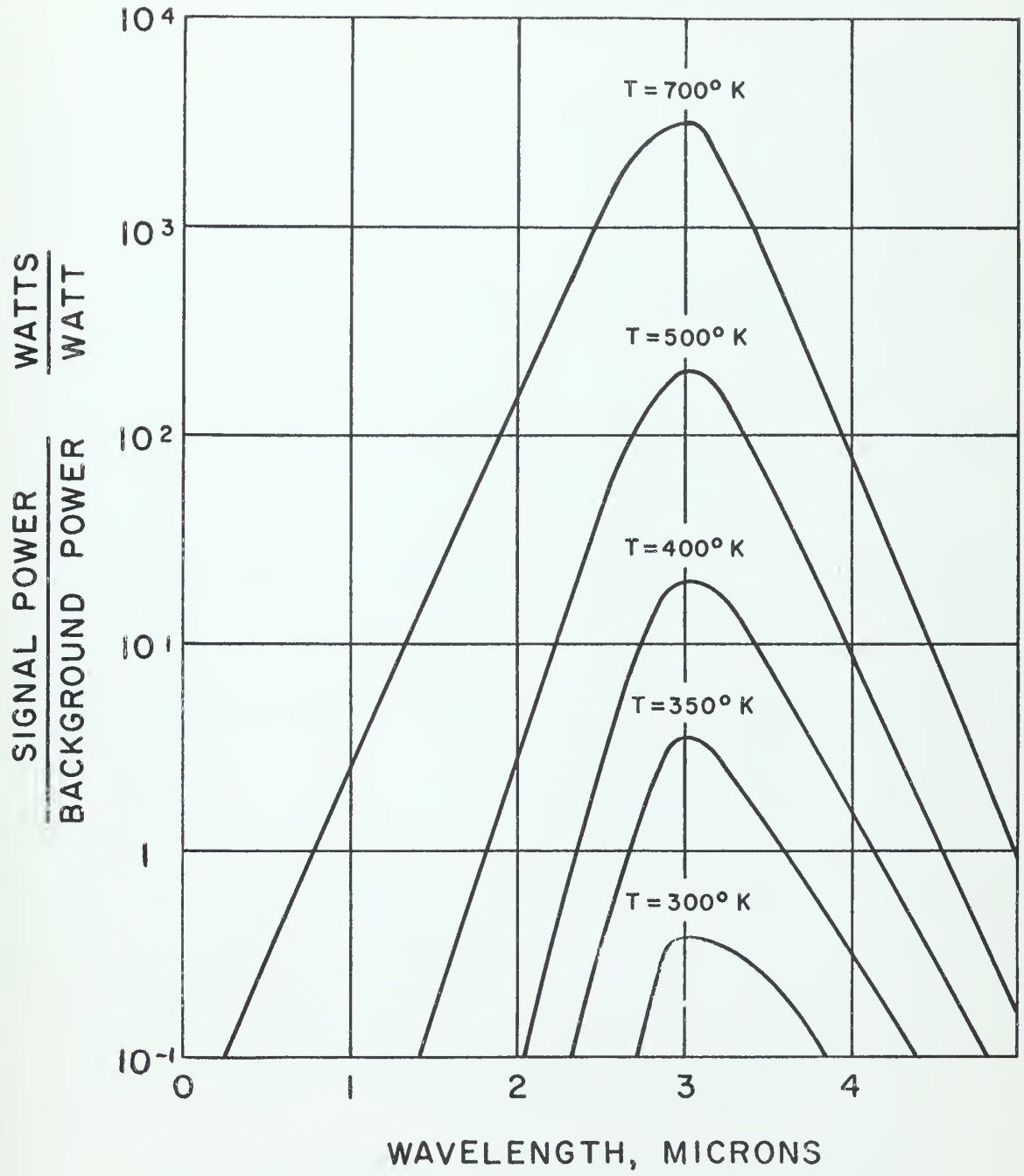

Figure 20. Ratio of Emitted Power to Extraneous Power Incident on the Detector Cell.

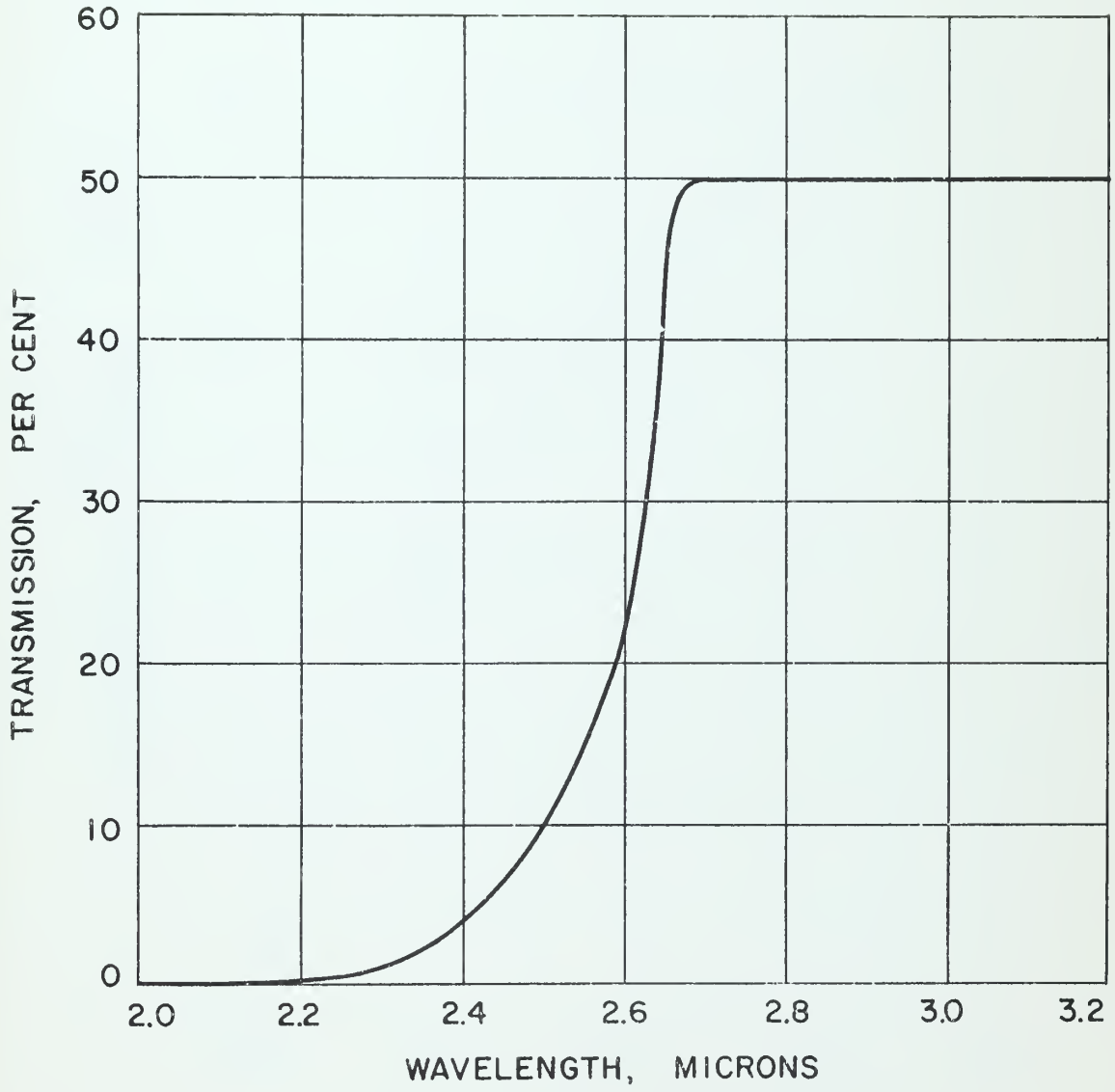

Figure 21. Desired Interference Filter Characteristics.

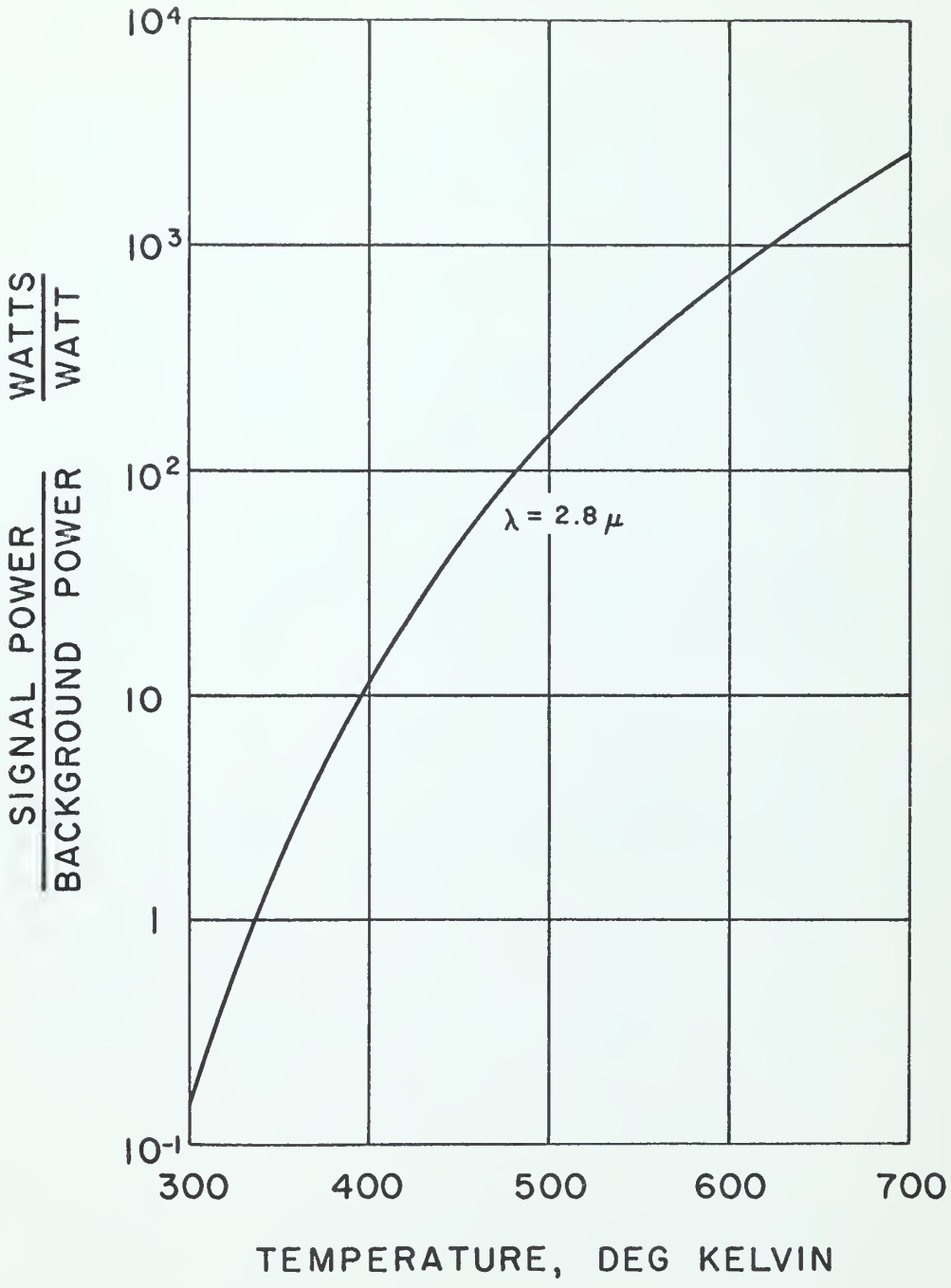

Figure 22. Ratio of Emitted Power to Extraneous Power Incident on the Detector Cell at a Wave Length of 2.8 Microns.

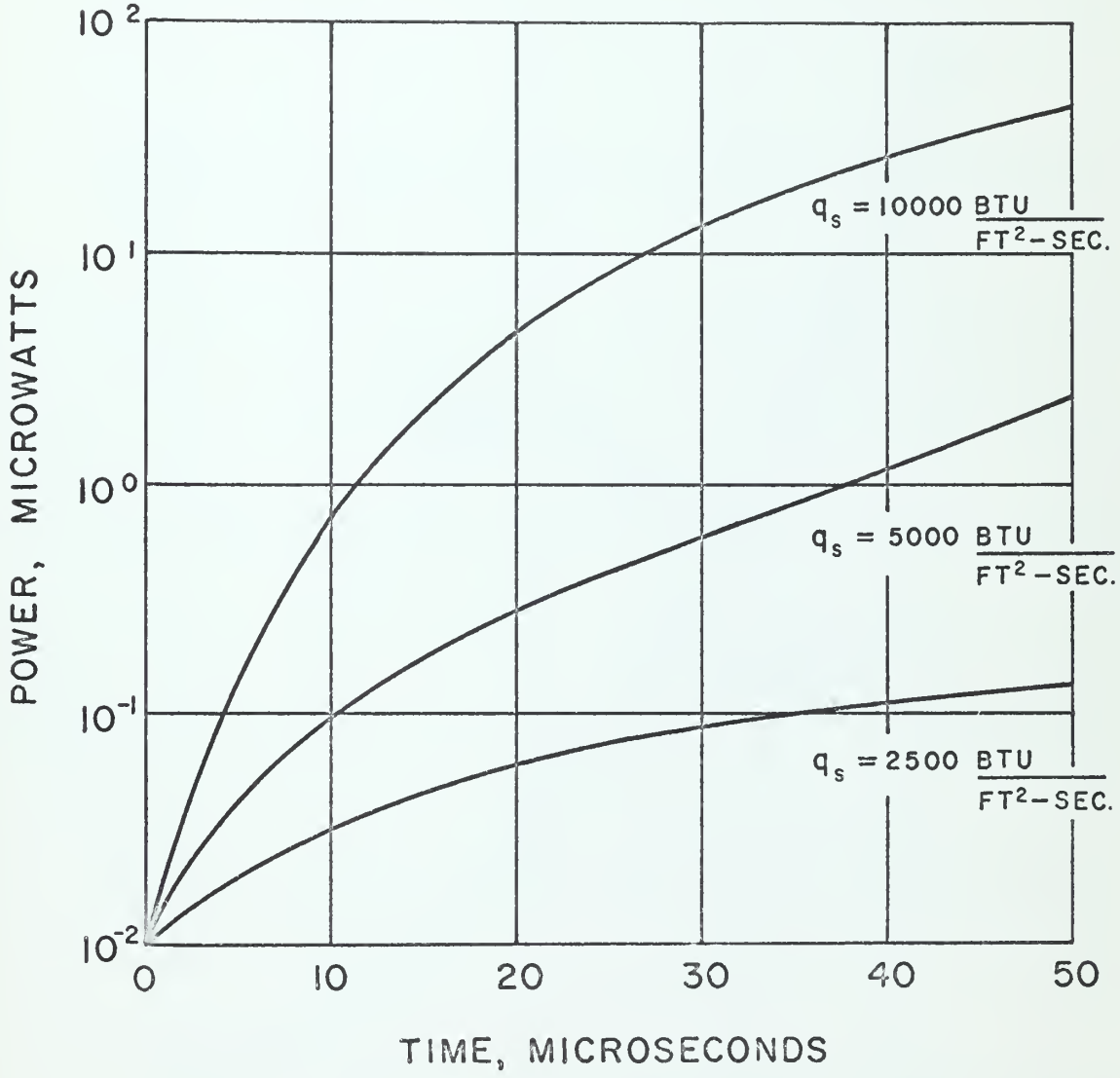

Figure 23. Incident Signal Power on the Detector Cell as a Function of Time and Heat Transfer Rate.

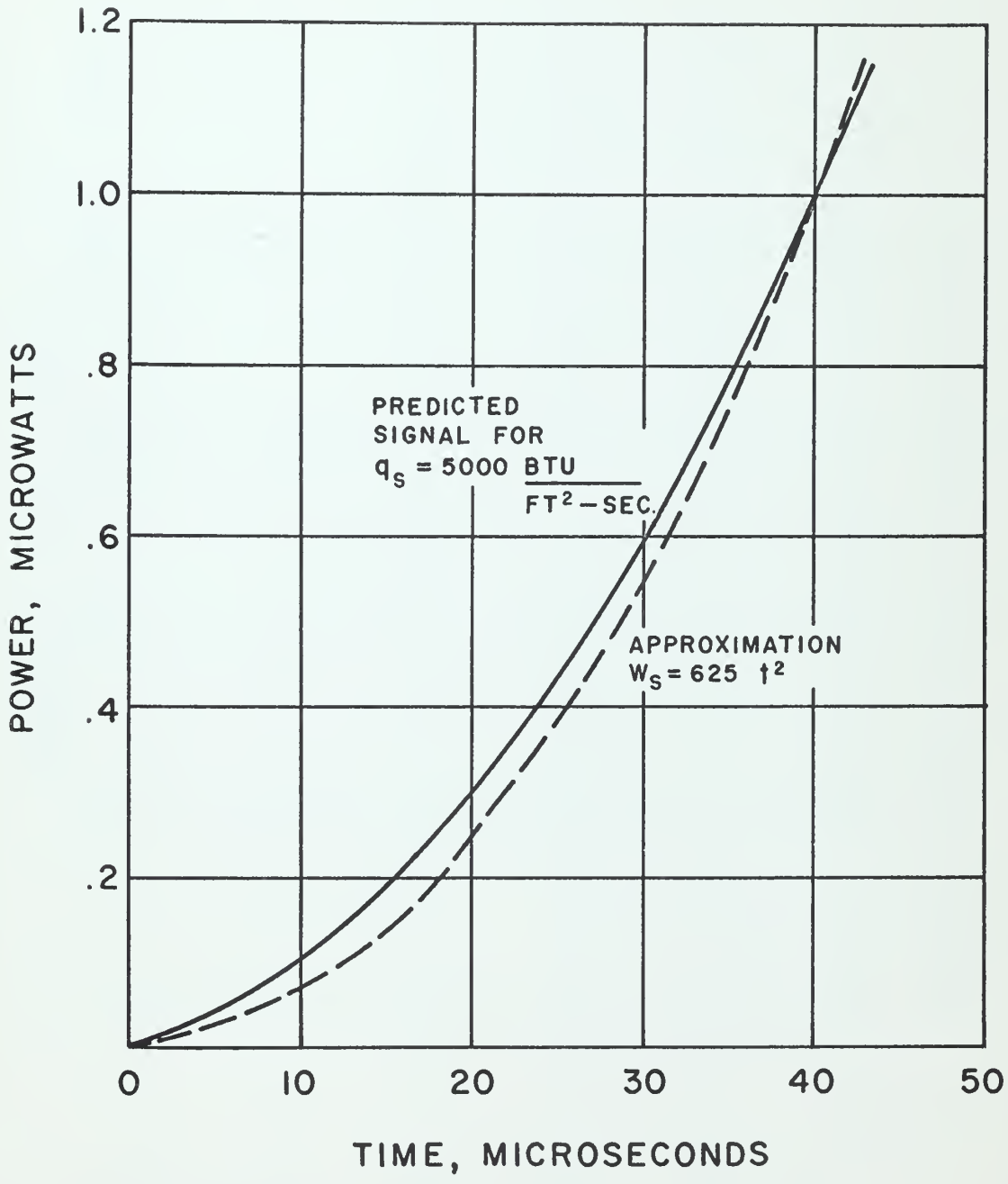

Figure 24. Approximating the Incident Power Relationship.

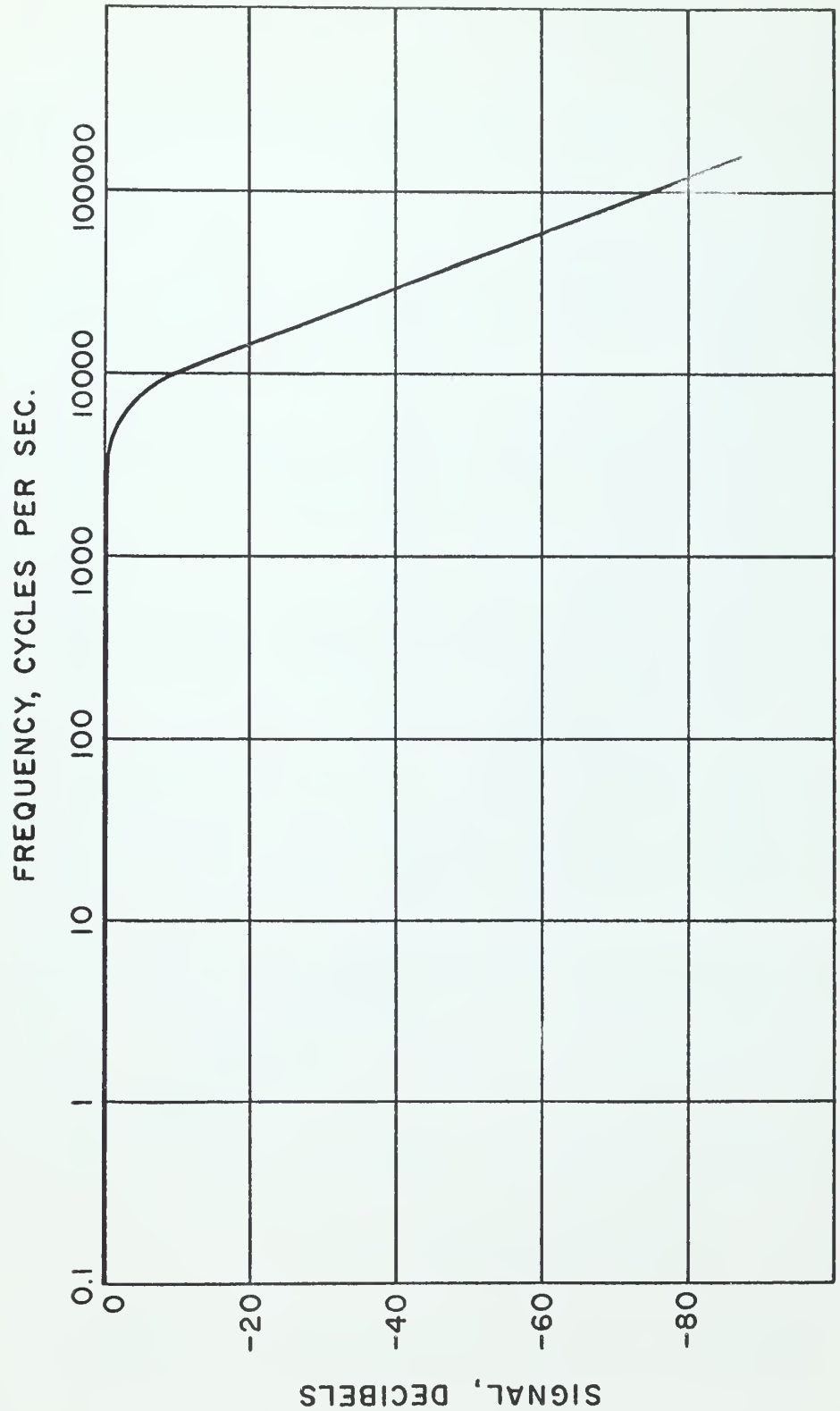

Figure 25. Amplifier Frequency Response Requirements.

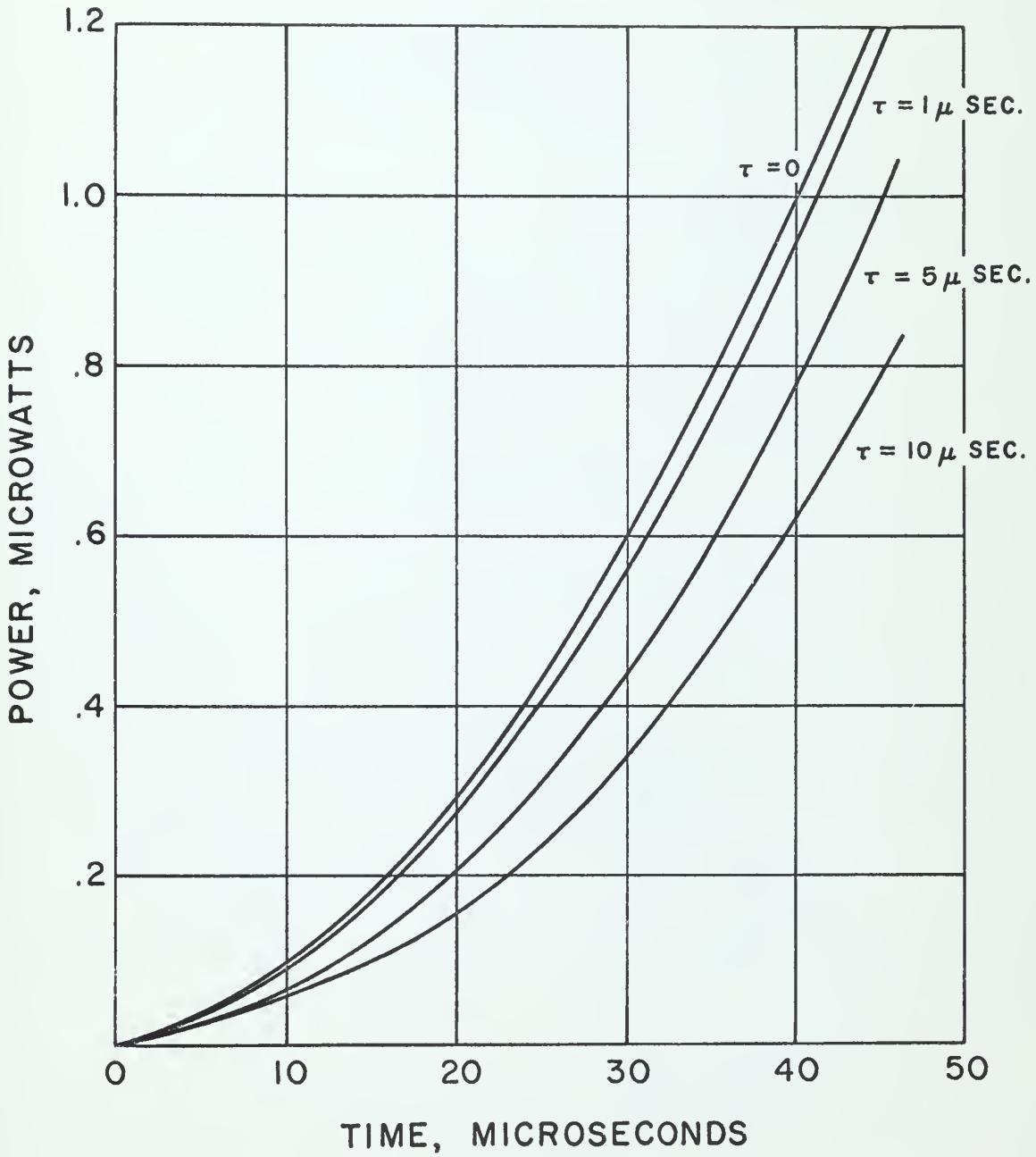

Figure 26. Detector Cell Time Constant Response.

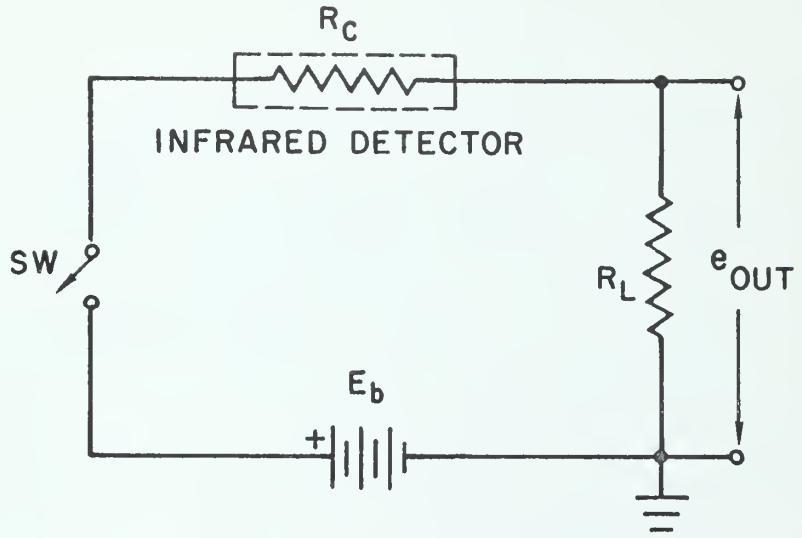

Series Circuit

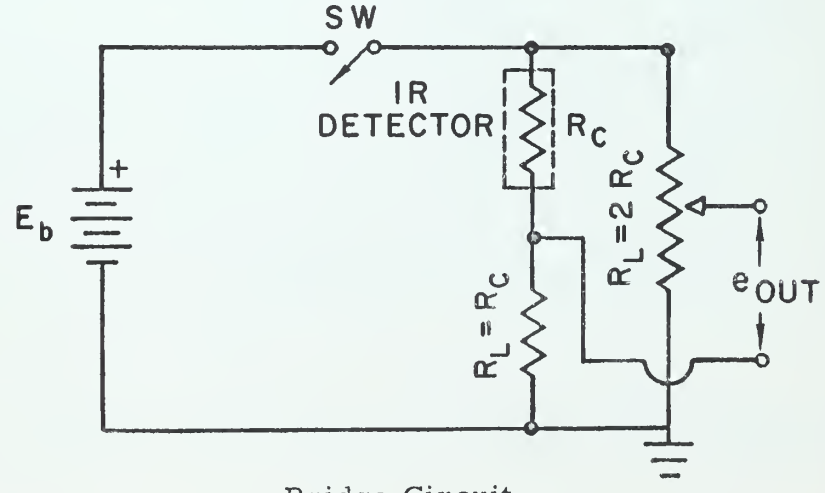

Bridge Circuit

Figure 27. Two Possible Detector Cell Circuits.

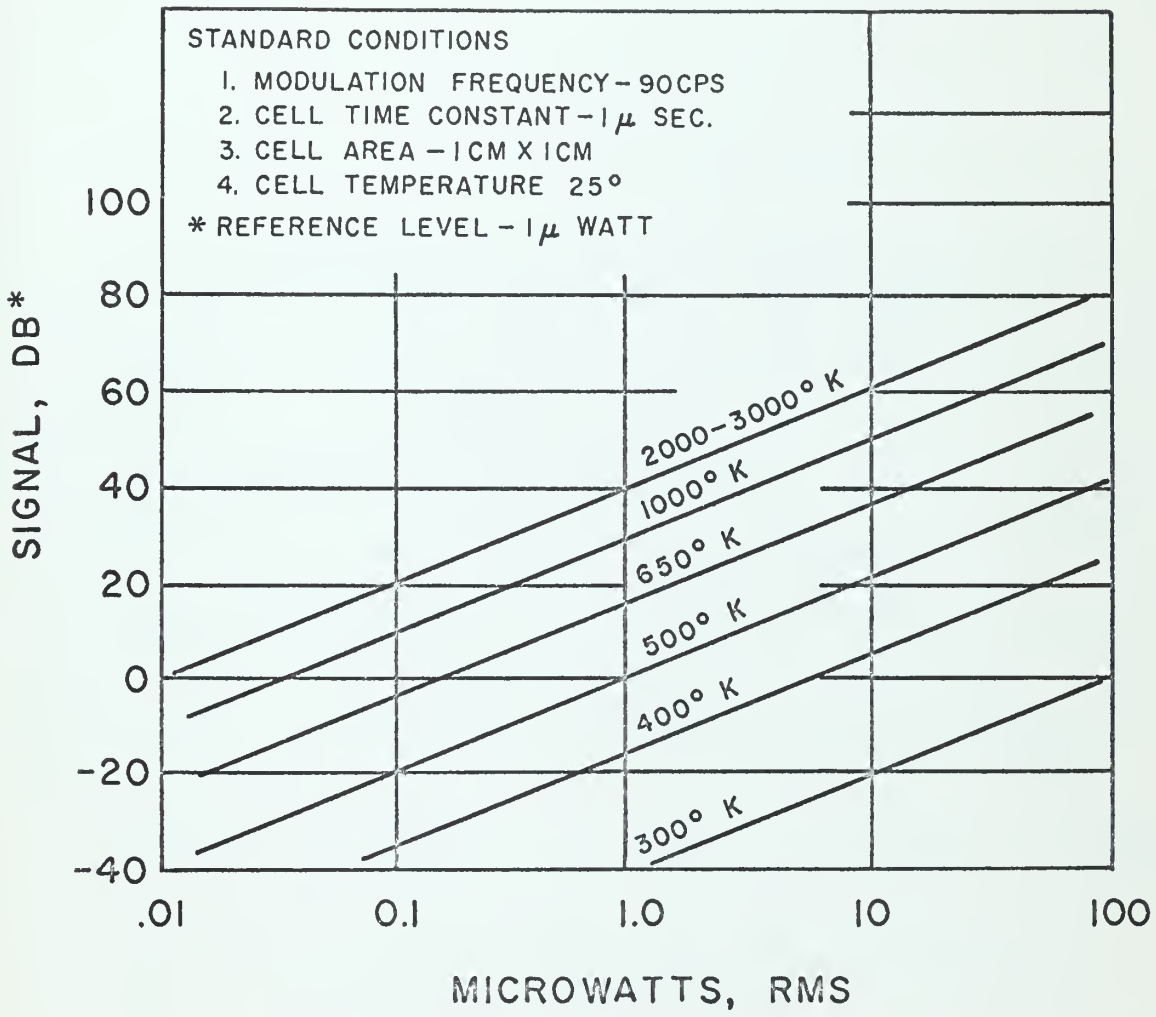

Figure 28. Typical Lead Sulphide Cell Responsivity Characteristics.

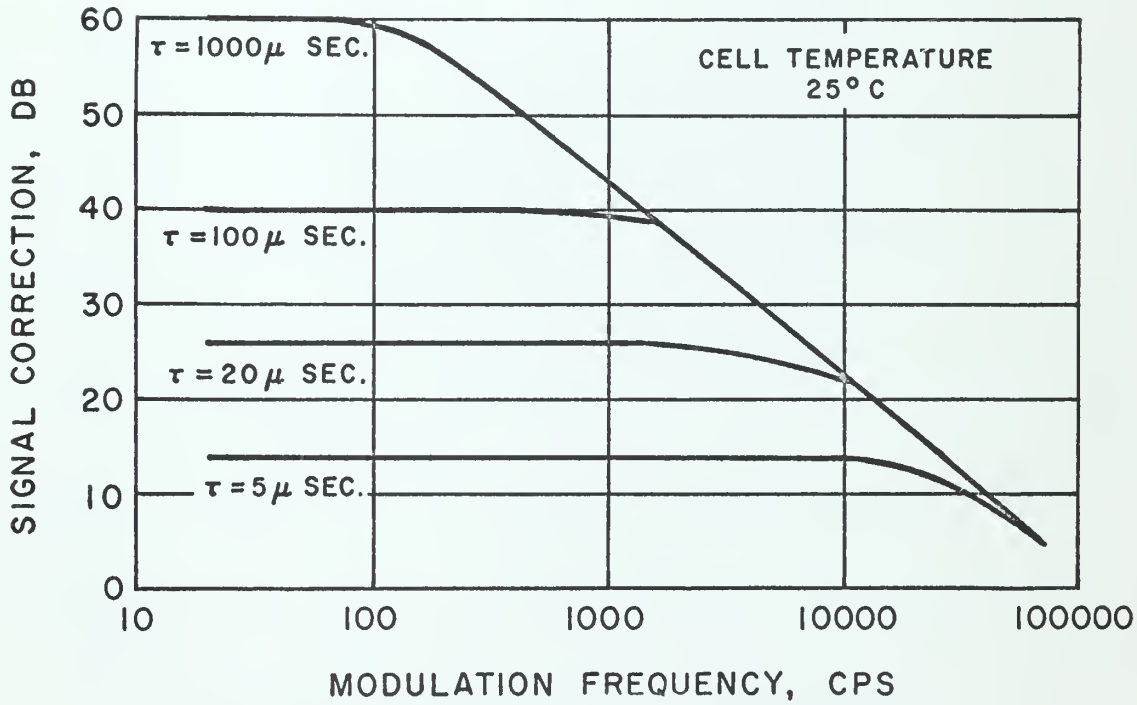

Figure 29. Correction to Responsivity Signal for Modulating Frequency and Time Constant.

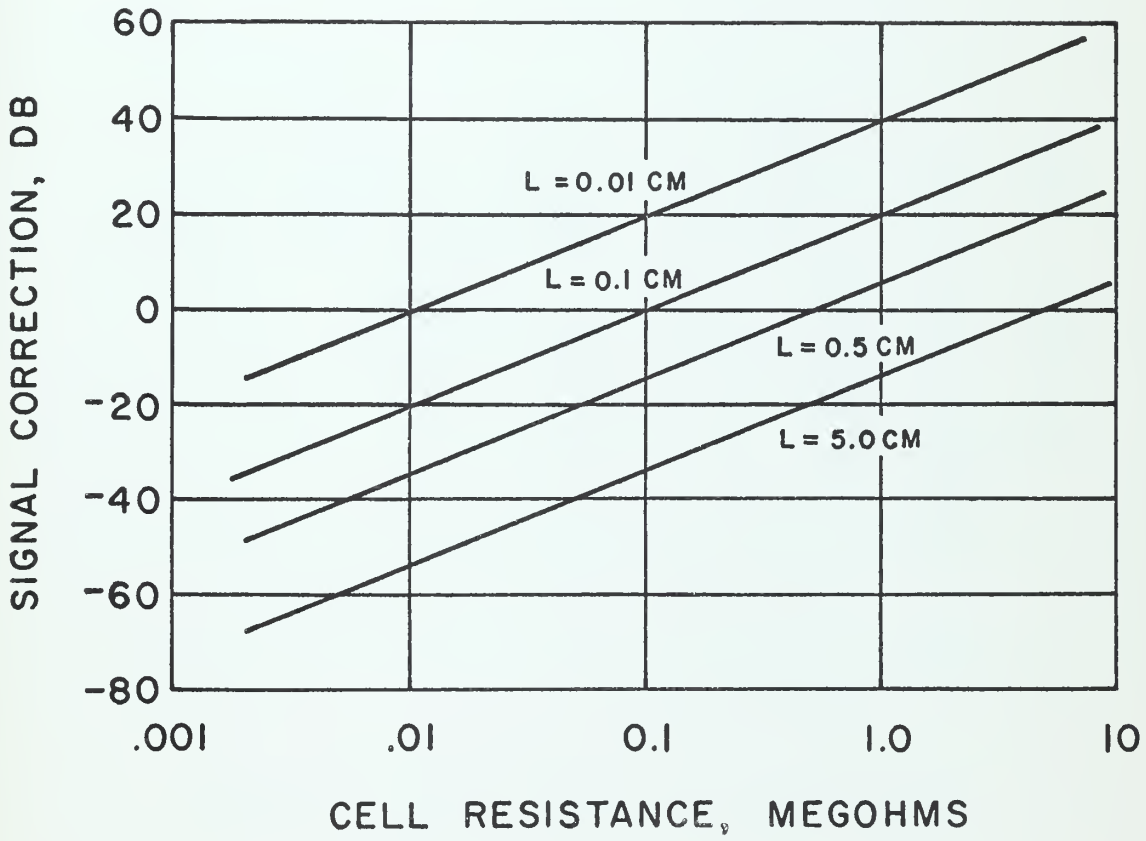

Figure 30. Correction to Responsivity Signal for Cell Area and Cell Resistance.

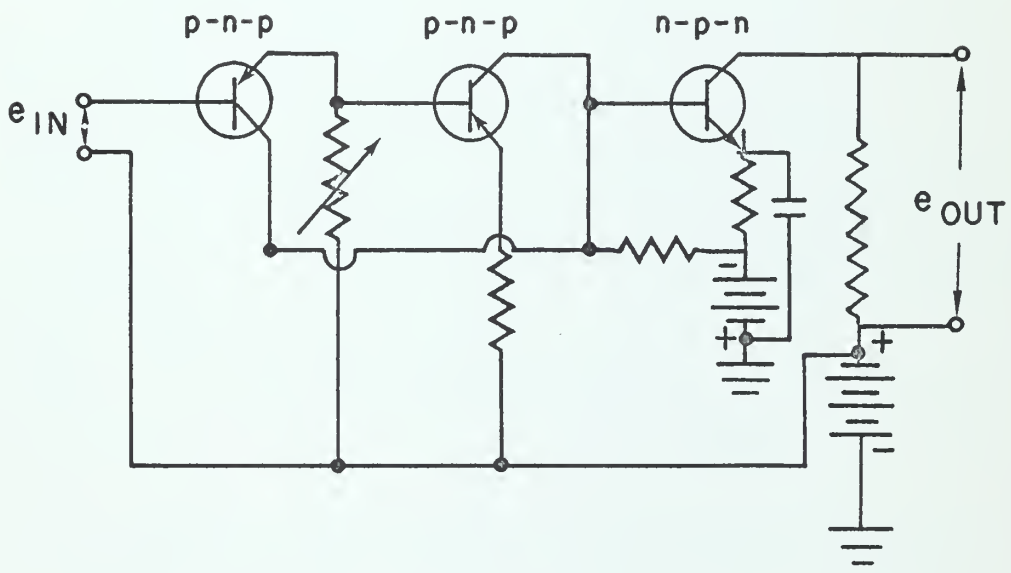

Figure 31. Direct-Coupled Transistor Amplifier.

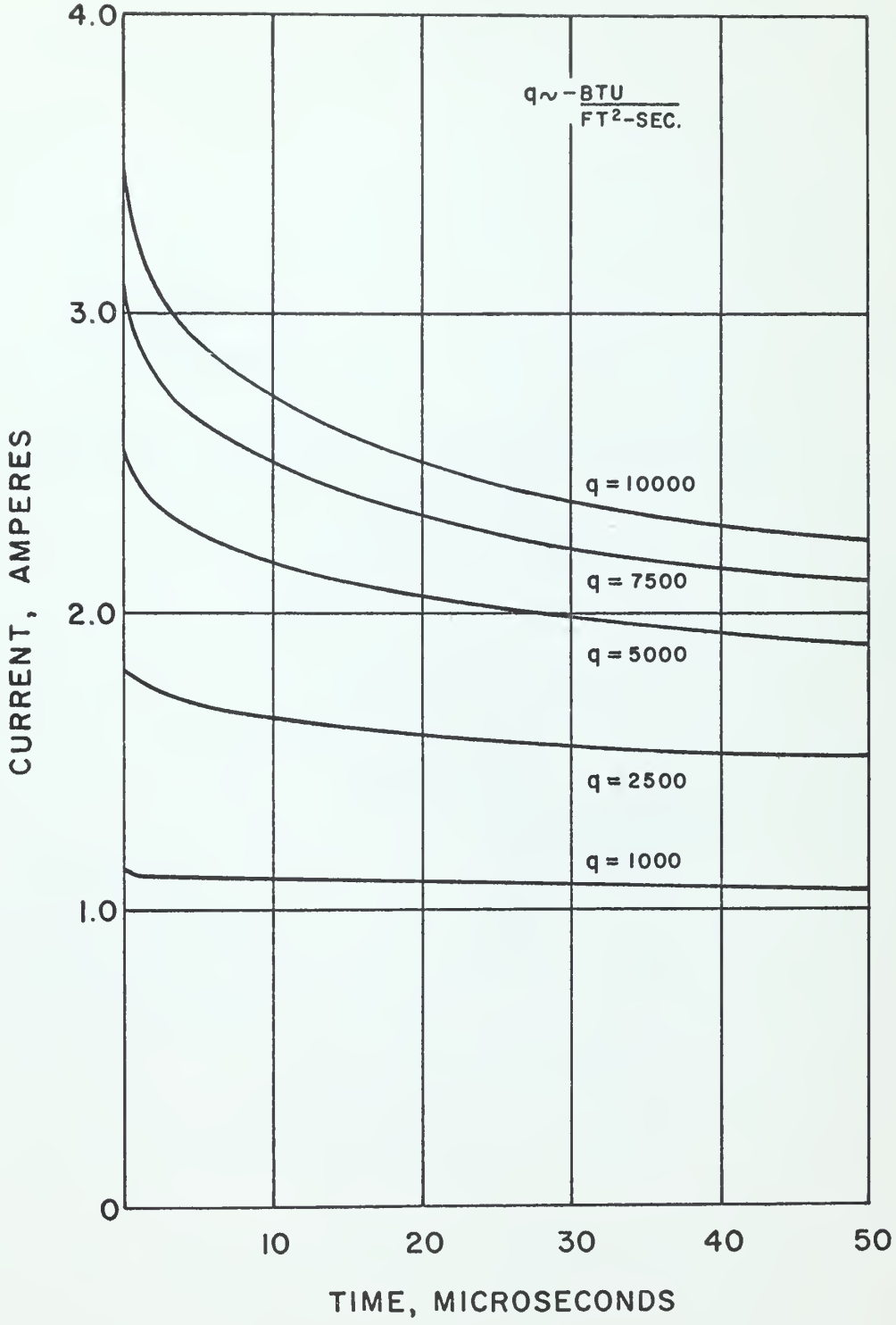

Figure 32. Calibration Current Pulse Requirements.

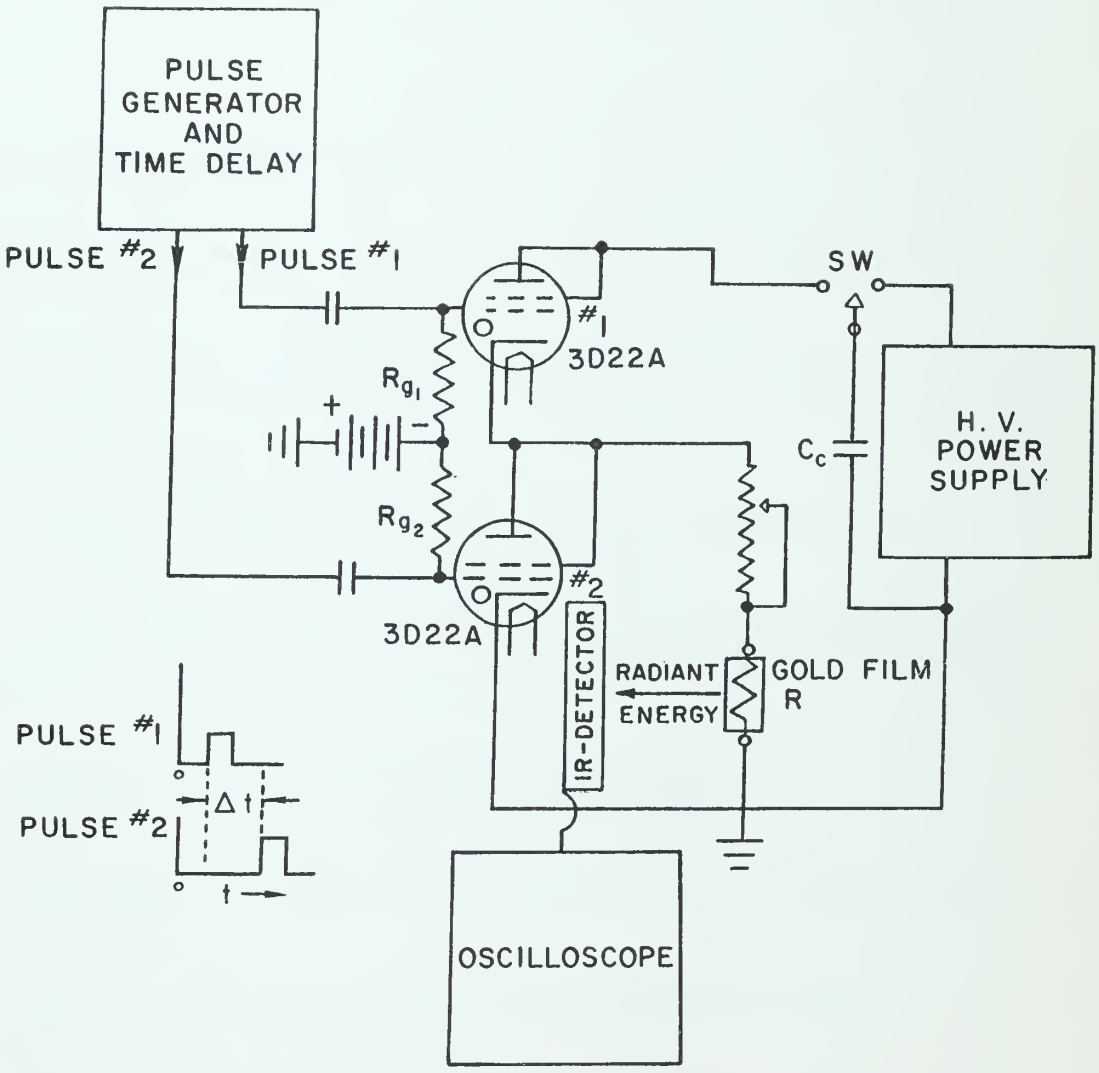

Figure 33. Proposed Calibration Circuit.

BIBLIOGRAPHY

R. G. Breckenridge, B. R. Russell and E. E. Hahn, Photoconductivity Conference, held at Atlantic City, November, 1954, John Wiley and Sons, Inc., New York, New York, 1956.

E. R. G. Eckert, Introduction to the Transfer of Heat and Mass, McGraw-Hill Book Company, Inc., New York, New York, 1950.

J. A. Fay and F. R. Riddell, Theory of Stagnation Point Heat Transfer in Dissociated Air, Avco Research Laboratory, RR-18, June, 1956 (revised April, 1957).

Saul Feldman, Hypersonic Gas Dynamic Charts for Equilibrium Air, Avco Research Laboratory, January, 1957.

N. H. Kemp and F. R. Riddell, Heat Transfer to Satellite Vehicles Re-entering the Atmosphere, Jet Propulsion, vol. 27, no. 2, part 1, p. 132, February, 1957.

J. F. Kinnard, Applied Electrical Measurements, John Wiley and Sons, Inc., New York, New York, 1956.

R. K. M. Landshoff, Magnetohydrodynamics, Stanford University Press, Stanford, California, 1957.

R. K. M. Landshoff, The Plasma in a Magnetic Field, Stanford University Press, Stanford, California, 1958.

H. W. Liepmann and A. E. Puckett, Introduction to Aerodynamics of a Compressible Fluid, John Wiley and Sons, Inc., New York, New York, 1947.

W. H. McAdams, Heat Transmission, Third Edition, McGraw-Hill Book Company, Inc., New York, New York, 1954.

H. O. McMahon, Thermal Radiation from Partially Transparent Reflecting Bodies, Journal of the Optical Society of America, vol. 40, no. 6, June, 1950.

H. T. Nagamatsu and R. E. Geiger, A Fast Response Device for Measuring Heat Transfer, General Engineering Laboratory, Schenectady, New York, May, 1957.

J. P. Raizer, On the Brightness of Strong Shock Waves in Air, Soviet Physics JETP, vol. 6, no. 1, January, 1958.

P. H. Rose and W. I. Stark, Stagnation Point Heat Transfer Measurements in Dissociated Air, Avco Research Laboratory, RR-24, revised April, 1957.

W. R. Sears, General Theory of High Speed Aerodynamics, High Speed Aerodynamics and Jet Propulsion, vol. 6, Princeton University Press, Princeton, New Jersey, 1954.

A. H. Shapiro, The Dynamics and Thermodynamics of Compressible Fluid Flow, vol. 1, Ronald Press Company, New York, New York, 1953.

R. F. Shea, Principles of Transistor Circuits, John Wiley and Sons, Inc., New York, New York, 1953.

W. E. Smith and R. J. Vidal, Some Problems Associated with Instrumenting Shock Tubes for Hypersonic Research, paper presented at ARS meeting in Buffalo, New York, September, 1956.

J. Strong, Procedures in Experimental Physics, Prentice-Hall, Inc., New York, New York, 1938.

F. E. Terman, Radio Engineering, Third Edition, McGraw-Hill Book Company, Inc., New York, New York, 1947.